6 Design

In the preceding chapters, we have discussed various aspects of fiber-reinforced polymers, including the constituent materials, mechanics, performance, and manufacturing methods. A number of unique characteristics of fiber-reinforced polymers that have emerged in these chapters are listed in Table 6.1. Many of these characteristics are due to the orthotropic nature of fiber-reinforced composites, which has also necessitated the development of new design approaches that are different from the design approaches traditionally used for isotropic materials, such as steel or aluminum alloys. This chapter describes some of the design methods and practices currently used for fiber-reinforced polymers including the failure prediction methods, the laminate design procedures, and the joint design considerations. A number of design examples are also included.

6.1 FAILURE PREDICTION

Design analysis of a structure or a component is performed by comparing stresses (or strains) due to applied loads with the allowable strength (or strain capacity) of the material. In the case of biaxial or multiaxial stress fields, a suitable failure theory is used for this comparison. For an isotropic material that exhibits yielding, such as a mild steel or an aluminum alloy, either the maximum shear stress theory or the distortional energy theory (von Mises yield criterion) is commonly used for designing against yielding. Fiber-reinforced polymers are not isotropic, nor do they exhibit gross yielding. Thus, failure theories developed for metals or other isotropic materials are not applicable to composite materials. Instead, many new failure theories have been proposed for fiber-reinforced composites, some of which are discussed in this section.

6.1.1 Failure Prediction in a Unidirectional Lamina

We consider the plane stress condition of a general orthotropic lamina containing unidirectional fibers at a fiber orientation angle of θ with respect to the x axis (Figure 6.1). In Chapter 3, we saw that four independent elastic constants, namely, E_{11}, E_{22}, G_{12}, and ν_{12}, are required to define its elastic characteristics. Its strength properties are characterized by five independent strength values:

S_{Lt} = longitudinal tensile strength
S_{Tt} = transverse tensile strength

TABLE 6.1
Unique Characteristics of Fiber-Reinforced Polymer Composites

Nonisotropic
- Orthotropic
- Directional properties
- Four independent elastic constants instead of two
- Principal stresses and principal strains not in the same direction
- Coupling between extensional and shear deformations

Nonhomogeneous
- More than one macroscopic constituent
- Local variation in properties due to resin-rich areas, voids, fiber misorientation, etc.
- Laminated structure

Laminated structure
- Extensional–bending coupling
- Planes of weakness between layers
- Interlaminar stresses
- Properties depend on the laminate type
- Properties may depend on stacking sequence
- Properties can be tailored according to requirements
- Poisson's ratio can be greater than 0.5

Nonductile behavior
- Lack of plastic yielding
- Nearly elastic or slightly nonelastic stress–strain behavior
- Stresses are not locally redistributed around bolted or riveted holes by yielding
- Low strains-to-failure in tension

Noncatastrophic failure modes
- Delamination
- Localized damage (fiber breakage, matrix cracking, debonding, fiber pullout, etc.)
- Less notch sensitivity
- Progressive loss in stiffness during cyclic loading
- Interlaminar shear failure in bending

Low coefficient of thermal expansion
- Dimensional stability
- Zero coefficient of thermal expansion possible
- Attachment problem with metals due to thermal mismatch

High internal damping: High attenuation of vibration and noise

Noncorroding

S_{Lc} = longitudinal compressive strength
S_{Tc} = transverse compressive strength
S_{LTs} = in-plane shear strength

Experimental techniques for determining these strength properties have been presented in Chapter 4. Note that the in-plane shear strength S_{LTs} in the principal material directions does not depend on the direction of the shear stress although both the longitudinal and transverse strengths may depend on the direction of the normal stress, namely, tensile or compressive.

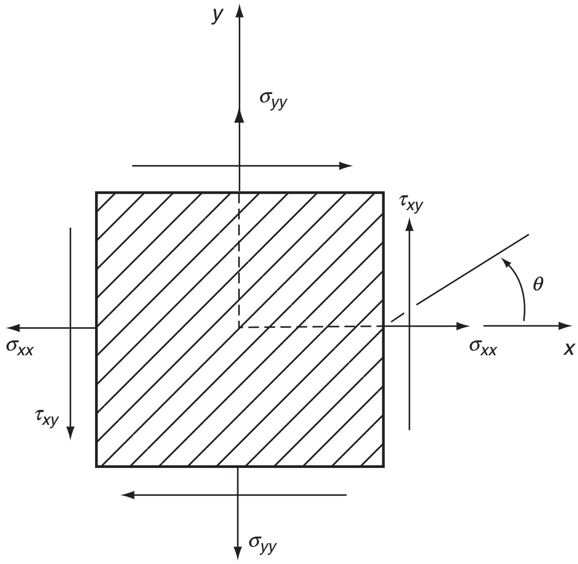

FIGURE 6.1 Two-dimensional stress state in a thin orthotropic lamina.

Many phenomenological theories have been proposed to predict failure in a unidirectional lamina under plane stress conditions. Among these, the simplest theory is known as the maximum stress theory; however, the more commonly used failure theories are the maximum strain theory and the Azzi–Tsai–Hill failure theory. We discuss these three theories as well as a more generalized theory, known as the Tsai–Wu theory. To use them, applied stresses (or strains) are first transformed into principal material directions using Equation 3.30. The transformed stresses are denoted σ_{11}, σ_{22}, and τ_{12}, and the applied stresses are denoted σ_{xx}, σ_{yy}, and τ_{xy}.

6.1.1.1 Maximum Stress Theory

According to the maximum stress theory, failure occurs when any stress in the principal material directions is equal to or greater than the corresponding ultimate strength. Thus to avoid failure,

$$\begin{aligned} -S_{\mathrm{Lc}} &< \sigma_{11} < S_{\mathrm{Lt}}, \\ -S_{\mathrm{Tc}} &< \sigma_{22} < S_{\mathrm{Tt}}, \\ -S_{\mathrm{LTs}} &< \tau_{12} < S_{\mathrm{LTs}}. \end{aligned} \tag{6.1}$$

For the simple case of uniaxial tensile loading in the x direction, only σ_{xx} is present and $\sigma_{\mathrm{yy}} = \tau_{xy} = 0$. Using Equation 3.30, the transformed stresses are

$$
\begin{aligned}
\sigma_{11} &= \sigma_{xx} \cos^2 \theta, \\
\sigma_{22} &= \sigma_{xx} \sin^2 \theta, \\
\tau_{12} &= -\sigma_{xx} \sin\theta \ \cos\theta.
\end{aligned}
$$

Thus, using the maximum stress theory, failure of the lamina is predicted if the applied stress σ_{xx} exceeds the smallest of $(S_{Lt}/\cos^2\theta)$, $(S_{Tt}/\sin^2\theta)$, and $(S_{LTs}/\sin\theta\ \cos\theta)$. Thus the safe value of σ_{xx} depends on the fiber orientation angle θ, as illustrated in Figure 6.2. At small values of θ, longitudinal tensile failure is expected, and the lamina strength is calculated from $(S_{Lt}/\cos^2\theta)$. At high values of θ, transverse tensile failure is expected, and the lamina strength is calculated from $(S_{Tt}/\sin^2\theta)$. At intermediate values of θ, in-plane shear failure of the lamina is expected and the lamina strength is calculated from $(S_{LTs}/\sin\theta\ \cos\theta)$. The change from longitudinal tensile failure to in-plane shear failure occurs at $\theta = \theta_1 = \tan^{-1} S_{LTs}/S_{Lt}$ and the change from in-plane shear failure to

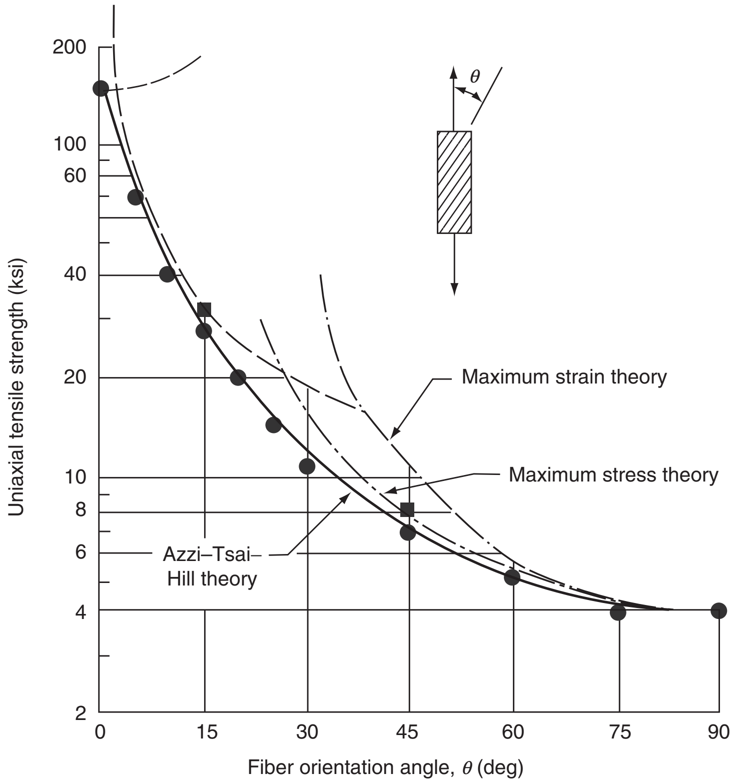

FIGURE 6.2 Comparison of maximum stress, maximum strain, and Azzi–Tsai–Hill theories with uniaxial strength data of a glass fiber-reinforced epoxy composite. (After Azzi, V.D. and Tsai, S.W., *Exp. Mech.*, 5, 283, 1965.)

transverse tensile failure occurs at $\theta = \theta_2 = \tan^{-1} S_{Tt}/S_{LTs}$. For example, for an E-glass fiber–epoxy composite with $S_{Lt} = 1100$ MPa, $S_{Tt} = 96.5$ MPa, and $S_{LTs} = 83$ MPa, $\theta_1 = 4.3°$ and $\theta_2 = 49.3°$. Thus, according to the maximum stress theory, longitudinal tensile failure of this composite lamina will occur for $0° \leq \theta < 4.3°$, in-plane shear failure will occur for $4.3° \leq \theta \leq 49.3°$ and transverse tensile failure will occur for $49.3° < \theta \leq 90°$.

EXAMPLE 6.1

A unidirectional continuous T-300 carbon fiber-reinforced epoxy laminate is subjected to a uniaxial tensile load P in the x direction. The laminate width and thickness are 50 and 2 mm, respectively. The following strength properties are known:

$$S_{Lt} = S_{Lc} = 1447.5 \text{ MPa},\ S_{Tt} = 44.8 \text{ MPa, and } S_{LTs} = 62 \text{ MPa}.$$

Determine the maximum value of P for each of the following cases: (a) $\theta = 0°$, (b) $\theta = 30°$, and (c) $\theta = 60°$.

Solution

The laminate is subjected to a uniaxial tensile stress σ_{xx} due to the tensile load applied in the x direction. In all three cases, $\sigma_{xx} = \frac{P}{A}$, where A is the cross-sectional area of the laminate.

1. Since $\theta = 0°$, $\sigma_{11} = \sigma_{xx}$, $\sigma_{22} = 0$, and $\tau_{12} = 0$.

   Therefore, in this case the laminate failure occurs when $\sigma_{11} = \sigma_{xx} = S_{Lt} = 1447.5$ MPa.

   Since $\sigma_{xx} = \frac{P}{A} = \frac{P}{(0.05 \text{ m})(0.002 \text{ m})}$, the tensile load P at which failure occurs is 144.75 kN. The mode of failure is the longitudinal tensile failure of the lamina.

2. Since $\theta = 30°$, using Equation 3.30,

$$\sigma_{11} = \sigma_{xx} \cos^2 30° = 0.75\ \sigma_{xx},$$
$$\sigma_{22} = \sigma_{xx} \sin^2 30° = 0.25\ \sigma_{xx},$$
$$\tau_{12} = \sigma_{xx} \sin 30° \cos 30° = 0.433\ \sigma_{xx}.$$

   According to Equation 6.1, the maximum values of σ_{11}, σ_{22}, and τ_{12} are

   (1) $\sigma_{11} = 0.75\sigma_{xx} = S_{Lt} = 1447.5$ MPa, which gives $\sigma_{xx} = 1930$ MPa
   (2) $\sigma_{22} = 0.25\sigma_{xx} = S_{Tt} = 44.8$ MPa, which gives $\sigma_{xx} = 179.2$ MPa
   (3) $\tau_{12} = 0.433\sigma_{xx} = S_{LTs} = 62$ MPa, which gives $\sigma_{xx} = 143.2$ MPa

   Laminate failure occurs at the lowest value of σ_{xx}. In this case, the lowest value is 143.2 MPa. Using $\sigma_{xx} = \frac{P}{A} = 143.2$ MPa, $P = 14.32$ kN. The mode of failure is the in-plane shear failure of the lamina.

3. Since $\theta = 60°$, using Equation 3.30,

$$\sigma_{11} = \sigma_{xx}\cos^2 60° = 0.25\ \sigma_{xx},$$
$$\sigma_{22} = \sigma_{xx}\sin^2 60° = 0.75\ \sigma_{xx},$$
$$\tau_{12} = \sigma_{xx}\sin 60° \cos 60° = 0.433\ \sigma_{xx}.$$

According to Equation 6.1, the maximum values of σ_{11}, σ_{22}, and τ_{12} are

(1) $\sigma_{11} = 0.25\sigma_{xx} = S_{\mathrm{Lt}} = 1447.5$ MPa, which gives $\sigma_{xx} = 5790$ MPa
(2) $\sigma_{22} = 0.75\sigma_{xx} = S_{\mathrm{Tt}} = 44.8$ MPa, which gives $\sigma_{xx} = 59.7$ MPa
(3) $\tau_{12} = 0.433\sigma_{xx} = S_{\mathrm{LTs}} = 62$ MPa, which gives $\sigma_{xx} = 143.2$ MPa

Laminate failure occurs at the lowest value of σ_{xx}. In this case, the lowest value is 59.7 MPa. Using $\sigma_{xx} = \frac{P}{A} = 59.7$ MPa, $P = 5.97$ kN. The mode of failure is transverse tensile failure of the lamina.

6.1.1.2 Maximum Strain Theory

According to the maximum strain theory, failure occurs when any strain in the principal material directions is equal to or greater than the corresponding ultimate strain. Thus to avoid failure,

$$-\varepsilon_{\mathrm{Lc}} < \varepsilon_{11} < \varepsilon_{\mathrm{Lt}},$$
$$-\varepsilon_{\mathrm{Tc}} < \varepsilon_{22} < \varepsilon_{\mathrm{Tt}},$$
$$-\gamma_{\mathrm{LTs}} < \gamma_{12} < \gamma_{\mathrm{LTs}}. \tag{6.2}$$

Returning to the simple case of uniaxial tensile loading in which a stress σ_{xx} is applied to the lamina, the safe value of this stress is calculated in the following way.

1. Using the strain–stress relationship, Equation 3.72, and the transformed stresses, the strains in the principal material directions are

$$\varepsilon_{11} = S_{11}\sigma_{11} + S_{12}\sigma_{22} = (S_{11}\cos^2\theta + S_{12}\sin^2\theta)\ \sigma_{xx},$$
$$\varepsilon_{22} = S_{12}\sigma_{11} + S_{22}\sigma_{22} = (S_{12}\cos^2\theta + S_{22}\sin^2\theta)\ \sigma_{xx},$$
$$\gamma_{12} = S_{66}\tau_{22} = -S_{66}\sin\theta\cos\theta\ \sigma_{xx},$$

where

$$S_{11} = \frac{1}{E_{11}}$$
$$S_{12} = -\frac{\nu_{12}}{E_{11}} = -\frac{\nu_{21}}{E_{22}}$$
$$S_{22} = \frac{1}{E_{22}}$$
$$S_{66} = \frac{1}{G_{12}}$$

2. Using the maximum strain theory, failure of the lamina is predicted if the applied stress σ_{xx} exceeds the smallest of

$$(1)\quad \frac{\varepsilon_{\mathrm{Lt}}}{S_{11}\cos^2\theta + S_{12}\sin^2\theta} = \frac{E_{11}\varepsilon_{\mathrm{Lt}}}{\cos^2\theta - \nu_{12}\sin^2\theta} = \frac{S_{\mathrm{Lt}}}{\cos^2\theta - \nu_{12}\sin^2\theta}$$

$$(2)\quad \frac{\varepsilon_{\mathrm{Tt}}}{S_{12}\cos^2\theta + S_{22}\sin^2\theta} = \frac{E_{22}\varepsilon_{\mathrm{Tt}}}{\sin^2\theta - \nu_{21}\cos^2\theta} = \frac{S_{\mathrm{Tt}}}{\sin^2\theta - \nu_{21}\cos^2\theta}$$

$$(3)\quad \frac{\gamma_{\mathrm{LTs}}}{S_{66}\sin\theta\cos\theta} = \frac{G_{12}\gamma_{\mathrm{LTs}}}{\sin\theta\cos\theta} = \frac{S_{\mathrm{LTs}}}{\sin\theta\cos\theta}$$

The safe value of σ_{xx} for various fiber orientation angles is also shown in Figure 6.2. It can be seen that the maximum strain theory is similar to the maximum stress theory for θ approaching 0°. Both theories are operationally simple; however, no interaction between strengths in different directions is accounted for in either theory.

EXAMPLE 6.2

A T-300 carbon fiber-reinforced epoxy lamina containing fibers at a + 10° angle is subjected to the biaxial stress condition shown in the figure. The following material properties are known:

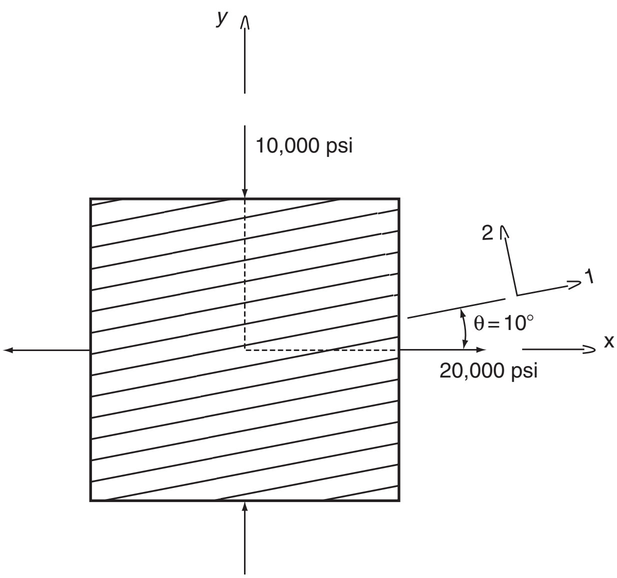

$$E_{11t} = E_{11c} = 21 \times 10^6 \text{ psi}$$
$$E_{22t} = 1.4 \times 10^6 \text{ psi}$$
$$E_{22c} = 2 \times 10^6 \text{ psi}$$
$$G_{12} = 0.85 \times 10^6 \text{ psi}$$
$$\nu_{12t} = 0.25$$
$$\nu_{12c} = 0.52$$
$$\varepsilon_{Lt} = 9{,}500 \ \mu\text{in./in.}$$
$$\varepsilon_{Tt} = 5{,}100 \ \mu\text{in./in.}$$
$$\varepsilon_{Lc} = 11{,}000 \ \mu\text{in./in.}$$
$$\varepsilon_{Tc} = 14{,}000 \ \mu\text{in./in.}$$
$$\gamma_{LTs} = 22{,}000 \ \mu\text{in./in.}$$

Using the maximum strain theory, determine whether the lamina would fail.

Solution

Step 1: Transform σ_{xx} and σ_{yy} into σ_{11}, σ_{22}, and τ_{12}.

$$\sigma_{11} = 20{,}000 \cos^2 10^\circ + (-10{,}000) \sin^2 10^\circ = 19{,}095.9 \text{ psi},$$
$$\sigma_{22} = 20{,}000 \sin^2 10^\circ + (-10{,}000) \cos^2 10^\circ = -9{,}095.9 \text{ psi},$$
$$\tau_{12} = (-20{,}000 - 10{,}000) \sin 10^\circ \cos 10^\circ = -5{,}130 \text{ psi}.$$

Step 2: Calculate ε_{11}, ε_{22}, and γ_{12}.

$$\varepsilon_{11} = \frac{\sigma_{11}}{E_{11t}} - \nu_{21c}\frac{\sigma_{22}}{E_{22c}} = 1134.3 \times 10^{-6} \text{ in./in.},$$
$$\varepsilon_{22} = -\nu_{12t}\frac{\sigma_{11}}{E_{11t}} + \frac{\sigma_{22}}{E_{22c}} = -4774.75 \times 10^{-6} \text{ in./in.},$$
$$\gamma_{12} = \frac{\tau_{12}}{G_{12}} = -6035.3 \times 10^{-6} \text{ in./in.}$$

Step 3: Compare ε_{11}, ε_{22}, and γ_{12} with the respective ultimate strains to determine whether the lamina has failed. For the given stress system in this example problem,

$$\varepsilon_{11} < \varepsilon_{Lt},$$
$$-\varepsilon_{Tc} < \varepsilon_{22},$$
$$-\gamma_{LTs} < \gamma_{12}.$$

Thus, the lamina has not failed.

6.1.1.3 Azzi–Tsai–Hill Theory

Following Hill's anisotropic yield criterion for metals, Azzi and Tsai [1] proposed that failure occurs in an orthotropic lamina if and when the following equality is satisfied:

$$\frac{\sigma_{11}^2}{S_{\mathrm{Lt}}^2} - \frac{\sigma_{11}\sigma_{22}}{S_{\mathrm{Lt}}^2} + \frac{\sigma_{22}^2}{S_{\mathrm{Tt}}^2} + \frac{\tau_{12}^2}{S_{\mathrm{LTs}}^2} = 1, \tag{6.3}$$

where σ_{11} and σ_{22} are both tensile (positive) stresses. When σ_{11} and σ_{22} are compressive, the corresponding compressive strengths are used in Equation 6.3.

For the uniaxial tensile stress situation considered earlier, failure is predicted if

$$\sigma_{xx} \geq \frac{1}{\left(\dfrac{\cos^4\theta}{S_{\mathrm{Lt}}^2} - \dfrac{\sin^2\theta\cos^2\theta}{S_{\mathrm{Lt}}^2} + \dfrac{\sin^4\theta}{S_{\mathrm{Tt}}^2} + \dfrac{\sin^2\theta\cos^2\theta}{S_{\mathrm{Lts}}^2}\right)^{1/2}}.$$

This equation, plotted in Figure 6.2, indicates a better match with experimental data than the maximum stress or the maximum strain theories.

EXAMPLE 6.3

Determine and draw the failure envelope for a general orthotropic lamina using Azzi–Tsai–Hill theory.

Solution

A failure envelope is a graphic representation of failure theory in the stress coordinate system and forms a boundary between the safe and unsafe design spaces. Selecting σ_{11} and σ_{22} as the coordinate axes and rearranging Equation 6.3, we can represent the Azzi–Tsai–Hill failure theory by the following equations.

1. In the $+\sigma_{11}/+\sigma_{22}$ quadrant, both σ_{11} and σ_{22} are tensile stresses. The corresponding strengths to consider are S_{Lt} and S_{Tt}.

$$\frac{\sigma_{11}^2}{S_{\mathrm{Lt}}^2} - \frac{\sigma_{11}\sigma_{22}}{S_{\mathrm{Lt}}^2} + \frac{\sigma_{22}^2}{S_{\mathrm{Tt}}^2} = 1 - \frac{\tau_{12}^2}{S_{\mathrm{LTs}}^2}$$

2. In the $+\sigma_{11}/-\sigma_{22}$ quadrant, σ_{11} is tensile and σ_{22} is compressive. The corresponding strengths to consider are S_{Lt} and S_{Tc}.

$$\frac{\sigma_{11}^2}{S_{\mathrm{Lt}}^2} + \frac{\sigma_{11}\sigma_{22}}{S_{\mathrm{Lt}}^2} + \frac{\sigma_{22}^2}{S_{\mathrm{Tc}}^2} = 1 - \frac{\tau_{12}^2}{S_{\mathrm{LTs}}^2}$$

3. In the $-\sigma_{11}/+\sigma_{22}$ quadrant, σ_{11} is compressive and σ_{22} is tensile. The corresponding strengths to consider are S_{Lc} and S_{Tt}.

$$\frac{\sigma_{11}^2}{S_{\mathrm{Lc}}^2}+\frac{\sigma_{11}\sigma_{22}}{S_{\mathrm{Lc}}^2}+\frac{\sigma_{22}^2}{S_{\mathrm{Tt}}^2}=1-\frac{\tau_{12}^2}{S_{\mathrm{LTs}}^2}$$

4. In the $-\sigma_{11}/-\sigma_{22}$ quadrant, both σ_{11} and σ_{22} are compressive stresses. The corresponding strengths to consider are S_{Lc} and S_{Tc}.

$$\frac{\sigma_{11}^2}{S_{\mathrm{Lc}}^2}-\frac{\sigma_{11}\sigma_{22}}{S_{\mathrm{Lc}}^2}+\frac{\sigma_{22}^2}{S_{\mathrm{Tc}}^2}=1-\frac{\tau_{12}^2}{S_{\mathrm{LTs}}^2}$$

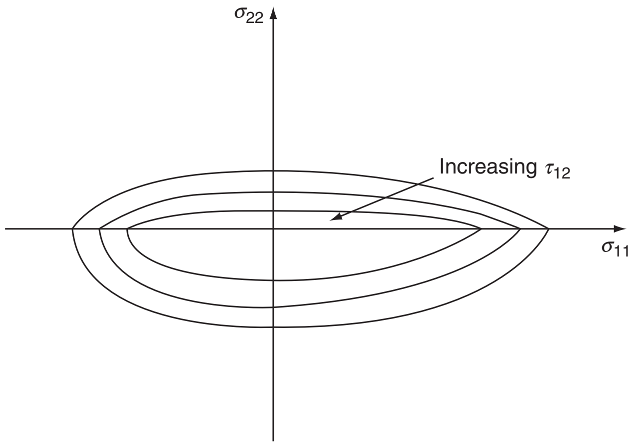

A failure envelope based on these equations is drawn in the figure for various values of the $\tau_{12}/S_{\mathrm{LTs}}$ ratio. Note that, owing to the anisotropic strength characteristics of a fiber-reinforced composite lamina, the Azzi–Tsai–Hill failure envelope is not continuous in the stress space.

6.1.1.4 Tsai–Wu Failure Theory

Under plane stress conditions, the Tsai–Wu failure theory [2] predicts failure in an orthotropic lamina if and when the following equality is satisfied:

$$F_1\sigma_{11}+F_2\sigma_{22}+F_6\tau_{12}+F_{11}\sigma_{11}^2+F_{22}\sigma_{22}^2+F_{66}\tau_{12}^2+2F_{12}\sigma_{11}\sigma_{22}=1, \quad (6.4)$$

where F_1, F_2, and so on are called the strength coefficients and are given by

$$
\begin{aligned}
F_1 &= \frac{1}{S_{\mathrm{Lt}}} - \frac{1}{S_{\mathrm{Lc}}} \\
F_2 &= \frac{1}{S_{\mathrm{Tt}}} - \frac{1}{S_{\mathrm{Tc}}} \\
F_6 &= 0 \\
F_{11} &= \frac{1}{S_{\mathrm{Lt}} S_{\mathrm{Lc}}} \\
F_{22} &= \frac{1}{S_{\mathrm{Tt}} S_{\mathrm{Tc}}} \\
F_{66} &= \frac{1}{S_{\mathrm{LTs}}^2}
\end{aligned}
$$

and F_{12} is a strength interaction term between σ_{11} and σ_{22}. Note that F_1, F_2, F_{11}, F_{22}, and F_{66} can be calculated using the tensile, compressive, and shear strength properties in the principal material directions. Determination of F_{12} requires a suitable biaxial test [3]. For a simple example, consider an equal biaxial tension test in which $\sigma_{11} = \sigma_{12} = \sigma$ at failure. Using Equation 6.4, we can write

$$(F_1 + F_2)\,\sigma + (F_{11} + F_{22} + 2F_{12})\,\sigma^2 = 1,$$

from which

$$F_{12} = \frac{1}{2\sigma^2}\left[1 - \left(\frac{1}{S_{\mathrm{Lt}}} - \frac{1}{S_{\mathrm{Lc}}} + \frac{1}{S_{\mathrm{Tt}}} - \frac{1}{S_{\mathrm{Tc}}}\right)\sigma - \left(\frac{1}{S_{\mathrm{Lt}} S_{\mathrm{Lc}}} + \frac{1}{S_{\mathrm{Tt}} S_{\mathrm{Tc}}}\right)\sigma^2\right].$$

Since reliable biaxial tests are not always easy to perform, an approximate range of values for F_{12} has been recommended [4]:

$$-\frac{1}{2}(F_{11}F_{22})^{1/2} \leq F_{12} \leq 0. \tag{6.5}$$

In the absence of experimental data, the lower limit of Equation 6.5 is frequently used for F_{12}.

Figure 6.3 shows a comparison of the maximum strain theory, the Azzi–Tsai–Hill Theory, and the Tsai–Wu theory with a set of experimental data for a carbon fiber–epoxy lamina. The Tsai–Wu theory appears to fit the data best, which can be attributed to the presence of the strength interaction terms in Equation 6.4. Note that, for a given value of τ_{12}, the failure envelope defined by the Tsai–Wu failure theory is a continuous ellipse in the (σ_{11}, σ_{22}) plane. The inclination of the ellipse in the σ_{11}, σ_{22} plane and the lengths of its semi-axes are controlled by the value of F_{12}. The ellipse intercepts the σ_{11} axis at S_{Lt} and $-S_{\mathrm{Lc}}$, and the σ_{22} axis at S_{Tt} and $-S_{\mathrm{Tc}}$.

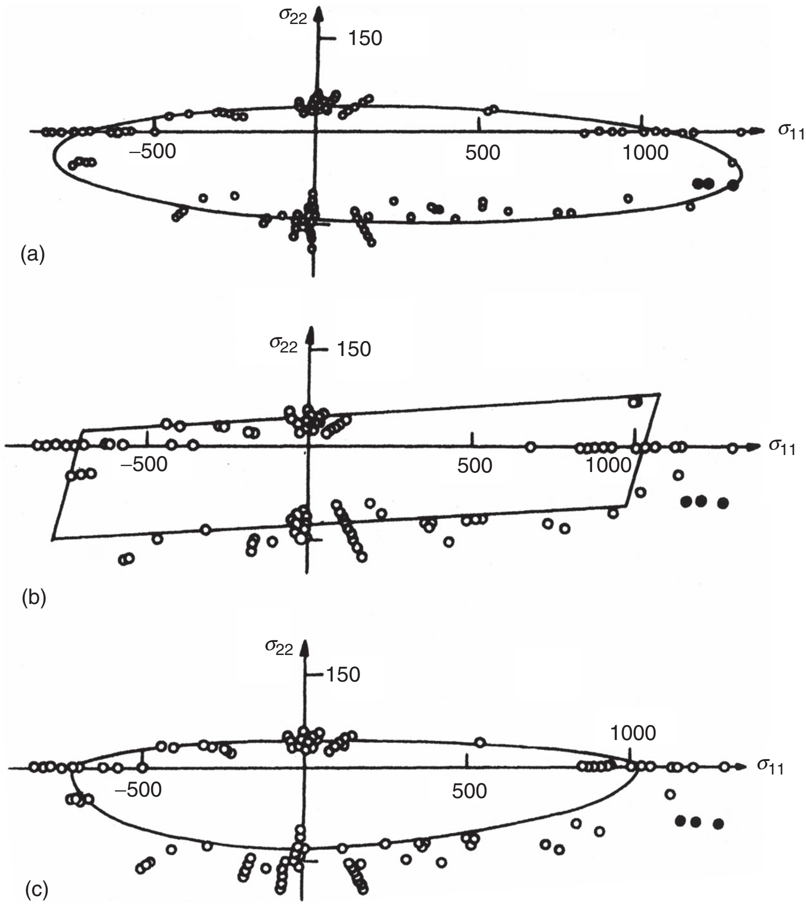

FIGURE 6.3 Comparison of (a) Tsai–Wu, (b) maximum strain, and (c) Azzi–Tsai–Hill failure theories with biaxial strength data of a carbon fiber-reinforced epoxy composite (note that the stresses are in MPa). (After Tsai, S.W. and Hahn, H.T., *Inelastic Behavior of Composite Materials*, C.T. Herakovich, ed., American Society of Mechanical Engineers, New York, 1975.)

EXAMPLE 6.4

Estimate the failure strength of a unidirectional lamina in an off-axis tension test using the Tsai–Wu theory. Assume that all strength coefficients for the lamina are known.

Solution

An off-axis tension test on a unidirectional lamina is performed at a fiber orientation angle θ with the loading axis. The stress state in the gage section of the lamina is shown in the figure. The stress σ_{xx} in the loading direction creates the following stresses in the principal material directions:

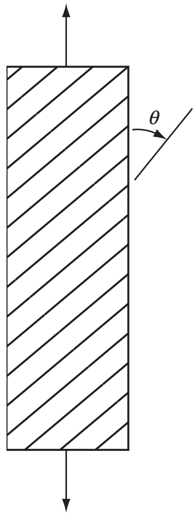

$$\sigma_{11} = \sigma_{xx}\cos^2\theta = \frac{1}{2}\sigma_{xx}(1+\cos 2\theta),$$
$$\sigma_{22} = \sigma_{xx}\sin^2\theta = \frac{1}{2}\sigma_{xx}(1-\cos 2\theta),$$
$$\tau_{12} = -\sigma_{xx}\sin\theta\cos\theta = -\frac{1}{2}\sigma_{xx}\sin 2\theta.$$

At failure, $\sigma_{xx} = S_\theta$, where S_θ denotes the failure strength in the off-axis tension test. Substituting for σ_{11}, σ_{22}, and τ_{12} in Equation 6.4 gives

$$S_\theta^2[(3F_{11}+3F_{22}+2F_{12}+F_{66})+4(F_{11}-F_{22})\cos 2\theta+(F_{11}+F_{22}-2F_{12}-F_{66})\cos 4\theta]+4S_\theta[(F_1+F_2)+(F_1-F_2)\cos 2\theta]-8=0.$$

This represents a quadratic equation of the form

$$AS_\theta^2 + BS_\theta + C = 0,$$

which can be solved to calculate the failure strength S_θ.

6.1.2 Failure Prediction for Unnotched Laminates

Failure prediction for a laminate requires knowledge of the stresses and strains in each lamina, which are calculated using the lamination theory described in Chapter 3. The individual lamina stresses or strains in the loading directions are transformed into stresses or strains in the principal material directions for each lamina, which are then used in an appropriate failure theory to check whether the lamina has failed. After a lamina fails, the stresses and strains in the remaining laminas increase and the laminate stiffness is reduced; however, the laminate may not fail immediately. Furthermore, the failed lamina may not cease to carry its share of load in all directions.

6.1.2.1 Consequence of Lamina Failure

Several methods have been proposed to account for the failed lamina and the subsequent behavior of the laminate [5]. Among them are the following:

Total discount method: In this method, zero stiffness and strength are assigned to the failed lamina in all directions.

Limited discount method: In this method, zero stiffness and strength are assigned to the failed lamina for the transverse and shear modes if the lamina failure is in the matrix material. If the lamina fails by fiber rupture, the total discount method is adopted.

Residual property method: In this method, residual strength and stiffness are assigned to the failed lamina.

EXAMPLE 6.5

A quasi-isotropic $[0/\pm45/90]_S$ laminate made from T-300 carbon–epoxy is subjected to an in-plane normal load N_{xx} per unit width. With increasing values of N_{xx}, failure occurs first in the 90° layers owing to transverse cracks.

Determine the stiffness matrices before and after the first ply failure (FPF). Assume that each ply has a thickness t_0. Use the same material properties as in Example 3.6.

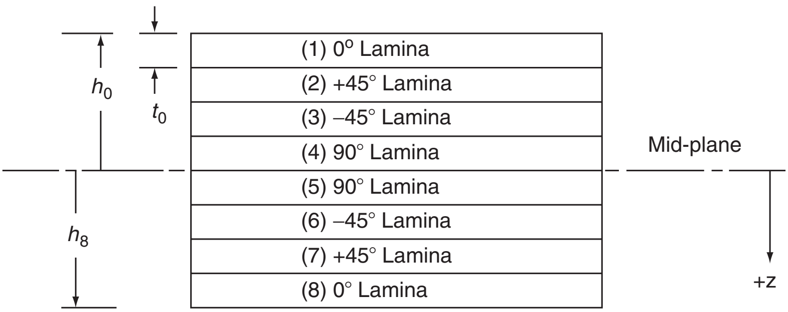

SOLUTIONS

Referring to the figure, we observe $h_8 = -h_0 = 4t_0$, $h_7 = -h_1 = 3t_0$, $h_6 = -h_2 = 2t_0$, $h_5 = h_3 = t_0$, and $h_4 = 0$. In addition, note that

$$
\begin{aligned}
(\bar{Q}_{mn})_1 &= (\bar{Q}_{mn})_8 = (\bar{Q}_{mn})_{0^\circ}, \\
(\bar{Q}_{mn})_2 &= (\bar{Q}_{mn})_7 = (\bar{Q}_{mn})_{+45^\circ}, \\
(\bar{Q}_{mn})_3 &= (\bar{Q}_{mn})_6 = (\bar{Q}_{mn})_{-45^\circ}, \\
(\bar{Q}_{mn})_4 &= (\bar{Q}_{mn})_5 = (\bar{Q}_{mn})_{90^\circ}.
\end{aligned}
$$

Since the given laminate is symmetric about the midplane, $[B] = [0]$. For in-plane loads, we need to determine the elements in the $[A]$ matrix.

$$\begin{aligned} A_{mn} &= \sum_{j=1}^{8} (\bar{Q}_{mn})_j (h_j - h_{j-1}) \\ &= 2t_0[(\bar{Q}_{mn})_{0^\circ} + (\bar{Q}_{mn})_{+45^\circ} + (\bar{Q}_{mn})_{-45^\circ} + (Q_{mn})_{90^\circ}]. \end{aligned}$$

Note that A_{mn} does not depend on the stacking sequence, since $(h_j - h_{j-1}) = t_0$ regardless of where the jth lamina is located.

Before the 90° layers fail: From Example 3.6, we tabulate the values of various $\bar{Q}_{mn}$ as follows. The unit of $\bar{Q}_{mn}$ is GPa.

	0°	**+45°**	**−45°**	**90°**
$\bar{Q}_{11}$	134.03	40.11	40.11	8.82
$\bar{Q}_{12}$	2.29	33.61	33.61	2.29
$\bar{Q}_{16}$	0	31.30	−31.30	0
$\bar{Q}_{22}$	8.82	40.11	40.11	134.03
$\bar{Q}_{26}$	0	31.30	−31.30	0
$\bar{Q}_{66}$	3.254	34.57	34.57	3.254

Therefore,

$$[A]_{\text{before}} = \begin{bmatrix} 446.14t_0 & 143.60t_0 & 0 \\ 143.60t_0 & 446.14t_0 & 0 \\ 0 & 0 & 151.30t_0 \end{bmatrix}.$$

After the 90° layers fail:

1. Total discount method: For the failed 90° layers, we assume $\bar{Q}_{11} = \bar{Q}_{12} = \bar{Q}_{16} = \bar{Q}_{22} = \bar{Q}_{26} = \bar{Q}_{66} = 0$.

   Therefore,

$$[A]_{\text{after}} = \begin{bmatrix} 428.50t_0 & 139.02t_0 & 0 \\ 139.02t_0 & 178.08t_0 & 0 \\ 0 & 0 & 144.79t_0 \end{bmatrix}$$

2. Limited discount method: Since the 90° layers failed by transverse cracking, we assume $\bar{Q}_{11} = \bar{Q}_{12} = \bar{Q}_{16} = \bar{Q}_{26} = \bar{Q}_{66} = 0$.

   However, $\bar{Q}_{22} = 134.03$ GPa. Therefore,

$$[A]_{\text{after}} = \begin{bmatrix} 428.50t_0 & 139.02t_0 & 0 \\ 139.02t_0 & 446.14t_0 & 0 \\ 0 & 0 & 144.79t_0 \end{bmatrix}$$

6.1.2.2 Ultimate Failure of a Laminate

Steps for the ultimate failure prediction of a laminate are as follows.

1. Calculate stresses and strains in each lamina using the lamination theory
2. Apply an appropriate failure theory to predict which lamina failed first
3. Assign reduced stiffness and strength to the failed lamina
4. Recalculate stresses and strains in each of the remaining laminas using the lamination theory
5. Follow through steps 2 and 3 to predict the next lamina failure
6. Repeat steps 2–4 until ultimate failure of the laminate occurs

Following the procedure outlined earlier, it is possible to generate failure envelopes describing the FPF as well as the ultimate failure of the laminate. In practice, a series of failure envelopes is drawn in a two-dimensional normal stress space in which the coordinate axes represent the average laminate stresses N_{xx}/h and N_{yy}/h. The area bounded by each failure envelope represents the safe design space for a constant average laminate shear stress N_{xy}/h (Figure 6.4).

Experimental verification for the laminate failure prediction methods requires the use of biaxial tests in which both normal stresses and shear stresses are present. Thin-walled large-diameter tubes subjected to various combinations of internal and external pressures, longitudinal loads, and torsional loads are the most suitable specimens for this purpose [6]. From the limited number of experimental results reported in the literature, it can be concluded

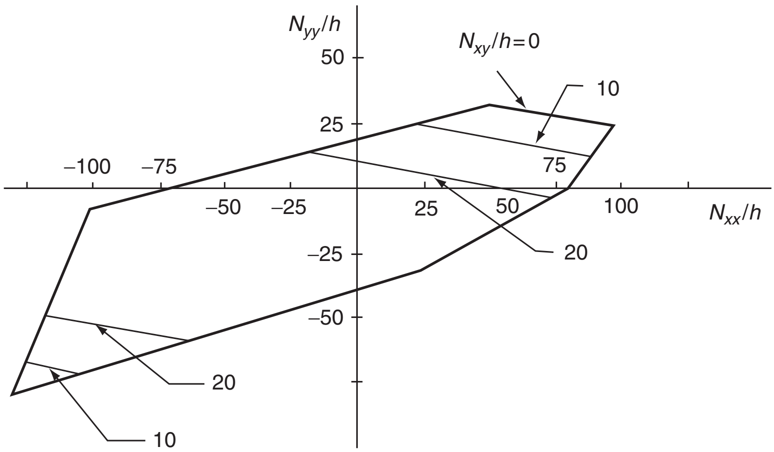

FIGURE 6.4 Theoretical failure envelopes for a carbon fiber–epoxy $[0/90\pm45]_S$ laminate (note that the in-plane loads per unit laminate thickness are in ksi).

that no single failure theory represents all laminates equally well. Among the various deficiencies in the theoretical prediction methods are the absence of interlaminar stresses and nonlinear effects. The assumption regarding the load transfer between the failed laminas and the active laminas can also introduce errors in the theoretical analyses.

The failure load prediction for a laminate depends strongly on the lamina failure theory selected [7]. In the composite material industry, there is little agreement on which lamina failure theory works best, although the maximum strain theory is more commonly used than the others [8]. Recently, the Tsai–Wu failure theory is finding more applications in the academic field.

6.1.3 Failure Prediction in Random Fiber Laminates

There are two different approaches for predicting failure in laminates containing randomly oriented discontinuous fibers.

In the Hahn's approach [9], which is a simple approach, failure is predicted when the maximum tensile stress in the laminate equals the following strength averaged over all possible fiber orientation angles:

$$S_r = \frac{4}{\pi}\sqrt{S_{Lt}S_{Tt}}, \tag{6.6}$$

where

S_r = strength of the random fiber laminate
S_{Lt} = longitudinal strength of a 0° laminate
S_{Tt} = transverse strength of a 0° laminate

In the Halpin–Kardos approach [10], the random fiber laminate is modeled as a quasi-isotropic $[0/\pm45/90]_S$ laminate containing discontinuous fibers in the 0°, ±45°, and 90° orientations. The Halpin–Tsai equations, Equations 3.49 through 3.53, are used to calculate the basic elastic properties, namely, E_{11}, E_{22}, ν_{12}, and G_{12}, of the 0° discontinuous fiber laminas. The ultimate strain allowables for the 0° and 90° laminas are estimated from the continuous fiber allowables using the Halpin–Kardos equations:

$$\varepsilon_{Lt(d)} = \varepsilon_{Lt}\left[\left(\frac{E_f}{E_m}\right)^{-0.87} + 0.50\right] \quad \text{for } l_f > l_c \tag{6.7}$$

and

$$\varepsilon_{Td(d)} = \varepsilon_{Tt}\left(1 - 1.21 v_f^{2/3}\right).$$

The procedure followed by Halpin and Kardos [10] for estimating the ultimate strength of random fiber laminates is the same as the ply-by-ply analysis used for continuous fiber quasi-isotropic $[0/\pm45/90]_S$ laminates.

6.1.4 Failure Prediction in Notched Laminates

6.1.4.1 Stress Concentration Factor

It is well known that the presence of a notch in a stressed member creates highly localized stresses at the root of the notch. The ratio of the maximum stress at the notch root to the nominal stress is called the stress concentration factor. Consider, for example, the presence of a small circular hole in an infinitely wide plate (i.e., $w \gg R$, Figure 6.5). The plate is subjected to a uniaxial tensile stress σ far from the hole. The tangential stress σ_{yy} at the two ends of the horizontal diameter of the hole is much higher than the nominal stress σ. In this case, the hole stress concentration factor K_T is defined as

$$K_T = \frac{\sigma_{yy}(R,0)}{\sigma}.$$

For an infinitely wide isotropic plate, the hole stress concentration factor is 3. For a symmetric laminated plate with orthotropic in-plane stiffness properties, the hole stress concentration factor is given by

$$K_T = 1 + \sqrt{\frac{2}{A_{22}}\left(\sqrt{A_{11}A_{22}} - A_{12} + \frac{A_{11}A_{22} - A_{12}^2}{2A_{66}}\right)}, \tag{6.8}$$

where A_{11}, A_{12},, A_{22}, and A_{66} are the in-plane stiffnesses defined in Chapter 3.

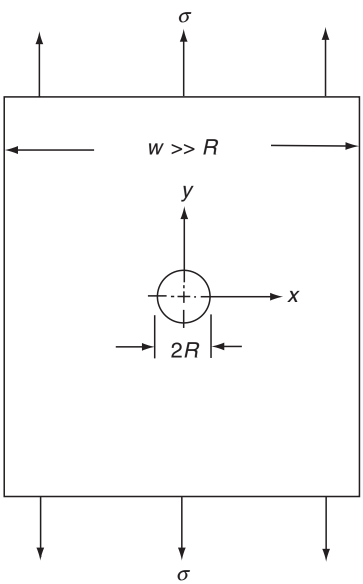

FIGURE 6.5 A uniaxially loaded infinite plate with a circular hole.

TABLE 6.2
Circular Hole Stress Concentration Factors

Material	Laminate	Circular Hole Stress Concentration Factor (K_T)
Isotropic material	—	3
S-glass–epoxy	0	4
	$[0_2/\pm 45]_S$	3.313
	$[0/90/\pm 45]_S$	3
	$[\pm 45]_S$	2.382
T-300 carbon–epoxy	0	6.863
	$[0_4/\pm 45]_S$	4.126
	$[0/90/\pm 45]_S$	3
	$[0/\pm 45]_S$	2.979
	$[\pm 45]_S$	1.984

Note that, for an infinitely wide plate, the hole stress concentration factor K_T is independent of the hole size. However, for a finite width plate, K_T increases with increasing ratio of hole diameter to plate width. No closed-form solutions are available for the hole stress concentration factors in finite width orthotropic plates. They are determined either by finite element methods [11,12] or by experimental techniques, such as strain gaging, moire interferometry, and birefringent coating, among other techniques [13]. Appendix A.7 gives the finite width correction factor for isotropic plates, which can be used for approximate calculation of hole stress concentration factors for orthotropic plates of finite width.

Table 6.2 lists values of hole stress concentration factors for a number of symmetric laminates. For each material, the highest value of K_T is observed with 0° fiber orientation. However, K_T decreases with increasing proportions of ±45° layers in the laminate. It is interesting to note that a $[0/90/\pm 45]_S$ laminate has the same K_T value as an isotropic material and a $[\pm 45°]_S$ laminate has a much lower K_T than an isotropic material.

6.1.4.2 Hole Size Effect on Strength

The hole stress concentration factor in wide plates containing very small holes ($R \leq w$) is constant, yet experimental results show that the tensile strength of many laminates is influenced by the hole diameter instead of remaining constant. This hole size effect has been explained by Waddoups et al. [14] on the basis of intense energy regions on each side of the hole. These energy regions were modeled as incipient cracks extending symmetrically from the hole boundary perpendicular to the loading direction. Later, Whitney and Nuismer [15,16] proposed two stress criteria to predict the strength of notched composites. These two failure criteria are discussed next.

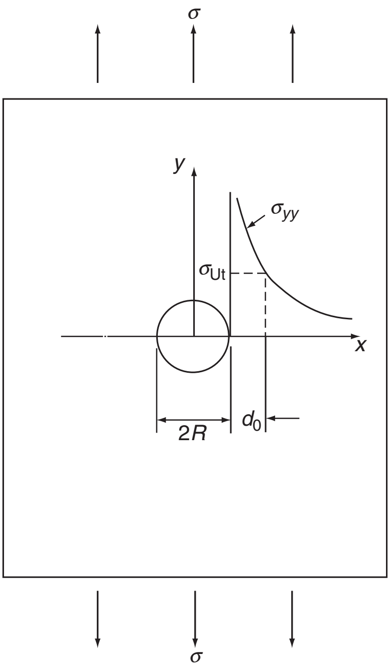

FIGURE 6.6 Failure prediction in a notched laminate according to the point stress criterion.

Point Stress Criterion: According to the point stress criterion, failure occurs when the stress over a distance d_0 away from the notch (Figure 6.6) is equal to or greater than the strength of the unnotched laminate. This characteristic distance d_0 is assumed to be a material property, independent of the laminate geometry as well as the stress distribution. It represents the distance over which the material must be critically stressed to find a flaw of sufficient length to initiate failure.

To apply the point stress criterion, the stress field ahead of the notch root must be known. For an infinitely wide plate containing a circular hole of radius R and subjected to a uniform tensile stress σ away from the hole, the most significant stress is σ_{yy} acting along the x axis on both sides of the hole edges. For an orthotropic plate, this normal stress component is approximated as [17]:

$$\sigma_{yy}(x,0) = \frac{\sigma}{2}\left\{2 + \left(\frac{R}{x}\right)^2 + 3\left(\frac{R}{x}\right)^4 - (K_\mathrm{T} - 3)\left[5\left(\frac{R}{x}\right)^6 - 7\left(\frac{R}{x}\right)^8\right]\right\}, \quad (6.9)$$

which is valid for $x \geq R$. In this equation, K_T is the hole stress concentration factor given in Equation 6.8.

According to the point stress criterion, failure occurs at $\sigma = \sigma_N$ for which

$$\sigma_{yy}(R + d_0, 0) = \sigma_{Ut},$$

where σ_N is the notched tensile strength and σ_{Ut} is the unnotched tensile strength for the laminate.

Thus from Equation 6.9, the ratio of notched to unnotched tensile strength is

$$\frac{\sigma_N}{\sigma_{Ut}} = \frac{2}{2 + \lambda_1^2 + 3\lambda_1^4 - (K_T - 3)(5\lambda_1^6 - 7\lambda_1^8)}, \tag{6.10}$$

where

$$\lambda_1 = \frac{R}{R + d_0}.$$

Average Stress Criterion: According to the average stress criterion, failure of the laminate occurs when the average stress over a distance a_0 ahead of the notch reaches the unnotched laminate strength. The characteristic distance a_0 is assumed to be a material property. It represents the distance over which incipient failure has taken place in the laminate owing to highly localized stresses.

In a plate containing a circular hole of radius R, failure by the average stress criterion occurs when

$$\frac{1}{a_0}\int_R^{R+a_0} \sigma_{yy}(x, 0)\mathrm{d}x = \sigma_{Ut}.$$

If the plate is made of a symmetric laminate with orthotropic properties, substitution of Equation 6.9 gives

$$\frac{\sigma_N}{\sigma_{Ut}} = \frac{2(1 - \lambda_2)}{2 - \lambda_2^2 - \lambda_2^4 + (K_T - 3)(\lambda_2^6 - \lambda_2^8)}, \tag{6.11}$$

where

$$\lambda_2 = \frac{R}{R + a_0}.$$

Both Equations 6.10 and 6.11 show that the notched tensile strength σ_N decreases with increasing hole radius. At very small hole radius, that is, as $R \to 0$, $\sigma_N \to \sigma_{Ut}$. At very large hole radius, as λ_1 or $\lambda_2 \to 1$, $\sigma_N \to \frac{\sigma_{Ut}}{K_T}$.

The following points should be noted in applying the point stress and the average stress criteria for notched laminates.

1. The application of both the criteria requires the knowledge of the overall stress field surrounding the notch tip. Since closed-form solutions are seldom available for notch geometries other than circular holes, this stress field must be determined by either numerical or experimental methods.
2. As a first approximation, the characteristic lengths d_0 and a_0 appearing in Equations 6.10 and 6.11 are considered independent of the notch geometry and the laminate configuration. Thus, the values d_0 and a_0 determined from a single hole test on one laminate configuration can be used for predicting the notched laminate strength of any laminate of the same material system. Nuismer and Whitney [16] have observed that $d_0 = 1.02$ mm (0.04 in.) and $a_0 = 3.81$ mm (0.15 in.) are applicable for a variety of laminate configurations of both E-glass fiber–epoxy and T-300 carbon fiber–epoxy composites.
3. Both the failure criteria make adequate failure predictions for notched laminates under uniaxial loading conditions only. The point stress criterion is simpler to apply than the average stress criterion. However, the errors resulting from the approximate analysis of the notch tip stresses tend to have less effect on the average stress criterion because of the averaging process itself.

It is important to note that, for many laminates, the unnotched tensile strength is strongly affected by the stacking sequence and the notched tensile strength is relatively insensitive to the stacking sequence. An example of this behavior is given in Table 6.3. In uniaxial tensile loading, unnotched $[\pm 45/90/0]_S$

TABLE 6.3
Tensile Strengths of Unnotched and Notched Laminates[a]

	Average Tensile Strength, MPa (ksi)	
Test Condition	$[\pm 45/0/90]_S$	$[90/0/\pm 45]_S$
Unnotched	451 (65.4)	499.3 (72.4)
Notched		
2.5 mm (0.1 in.) hole	331.7 (48.1)	322.8 (46.8)
7.5 mm (0.3 in.) hole	273.1 (39.6)	273.1 (39.6)
15.0 mm (0.6 in.) hole	235.2 (34.1)	233.1 (33.8)
2.5 mm (0.1 in.) crack	324.2 (47.0)	325.5 (47.2)
7.5 mm (0.3 in.) crack	268.3 (38.9)	255.9 (37.1)
15.0 mm (0.6 in.) crack	222.1 (32.2)	214.5 (31.1)

Source: Adapted from Whitney, J.M. and Kim, R.Y., *Composite Materials: Testing and Design* (*Fourth Conference*), *ASTM STP,* 617, 229, 1977.

[a] Material: T-300 carbon–epoxy.

laminates fail by gross edge delaminations due to the presence of tensile interlaminar normal stress σ_{zz} throughout the thickness. In contrast, the interlaminar normal stress at the free edges of $[90/0/\pm 45]_S$ laminates under similar loading conditions is compressive in nature and no free-edge delaminations are found in these laminates. When notched, both laminates fail by the initiation and propagation of tensile cracks from the hole boundary, regardless of the interlaminar stress distributions at the free edges of the hole or the straight boundaries.

EXAMPLE 6.6

Failure Prediction in a Centrally Cracked Plate. Using the point stress criterion, estimate the strength of an infinitely wide symmetric laminated plate containing a central straight crack of length $2c$ subjected to a uniform tensile stress applied normal to the crack plane at infinity.

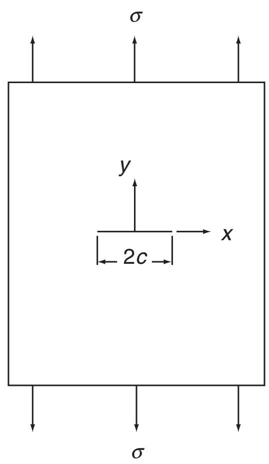

Solution

The expression for the normal stress σ_{yy} ahead of the crack is

$$\sigma_{yy}(x, 0) = \frac{x}{\sqrt{x^2 - c^2}}\sigma,$$

which is valid for $x > c$.

According to the point stress criterion, failure occurs at $\sigma = \sigma_N$ for which $\sigma_{yy}(c + d_0, 0) = \sigma_{Ut}$.

Thus,

$$\frac{(c + d_0)\sigma_N}{\sqrt{(c + d_0)^2 - c^2}} = \sigma_{Ut}$$

or

$$\sigma_{\mathrm{N}} = \sigma_{\mathrm{Ut}}\sqrt{1-\lambda_3^2},$$

where

$$\lambda_3 = \frac{c}{c+d_0}.$$

The mode I stress intensity factor for this condition can be written as

$$K_{\mathrm{I}} = \sigma_{\mathrm{N}}\sqrt{\pi c} = \sigma_{\mathrm{Ut}}\sqrt{\pi c(1-\lambda_3^2)}.$$

6.1.5 Failure Prediction for Delamination Initiation

Delamination or ply separation due to interlaminar stresses is a critical failure mode in many composite laminates. It can reduce the failure strength of some laminates well below that predicted by the in-plane failure theories discussed in Section 6.1.1.

Brewer and Lagace [18] as well as Zhou and Sun [19] proposed the following quadratic failure criterion to predict the initiation of delamination at the free edges:

$$\frac{\bar{\sigma}_{zz}^2}{S_{z\mathrm{t}}^2} + \frac{\bar{\tau}_{xz}^2}{S_{xz}^2} + \frac{\bar{\tau}_{yz}^2}{S_{yz}^2} = 1, \tag{6.12}$$

where

$S_{z\mathrm{t}}$ = tensile strength in the thickness direction
S_{xz}, S_{yz} = interlaminar shear strengths

$\bar{\sigma}_{zz}$, $\bar{\tau}_{xz}$, and $\bar{\tau}_{yz}$ are the average interlaminar stresses defined by

$$(\bar{\sigma}_{zz}, \bar{\tau}_{xz}, \bar{\tau}_{yz}) = \frac{1}{x_{\mathrm{c}}}\int_0^{x_{\mathrm{c}}} (\sigma_{zz}, \tau_{xz}, \tau_{yz})\mathrm{d}x,$$

where x_{c} is the critical distance over which the interlaminar stresses are averaged.

Since the interlaminar strength data are not usually available, Zhou and Sun [19] have suggested using $S_{xz} = S_{yz} = S_{\mathrm{LTs}}$ and $S_{z\mathrm{t}} = S_{\mathrm{Tt}}$.. They also recommend using x_{c} equal to twice the ply thickness.

EXAMPLE 6.7

The average interlaminar shear stresses in a $[\pm 45]_{2\mathrm{S}}$ laminate under an in-plane tensile force $N_{xx} = 410$ kN/m are given as:

Interface	$\bar{\sigma}_{zz}$ (MPa)	$\bar{\tau}_{xz}$ (MPa)	$\bar{\tau}_{yz}$ (MPa)
1	−0.9	−5.67	68.71
2	−1.45	−2.71	26.60
3	0.73	9.91	67.47

Using $S_{zt} = 42.75$ MPa and $S_{xz} = S_{yz} = 68.95$ MPa, investigate whether any of the interfaces will fail by delamination at this load.

Solution

Interface 1: Since $\bar{\sigma}_{zz}$ is compressive, we will not consider it in the failure prediction by Equation 6.12. Thus, the left-hand side (LHS) of Equation 6.12 is

$$\left(\frac{-5.67}{68.95}\right)^2 + \left(\frac{68.71}{68.95}\right)^2 \approx 1.$$

Interface 2: The term $\bar{\sigma}_{zz}$ is also compressive at this interface. Therefore, we will not consider σ_{zz} in the failure prediction by Equation 6.12. Thus the LHS of Equation 6.12 is

$$\left(\frac{-2.71}{68.95}\right)^2 + \left(\frac{26.6}{68.95}\right)^2 = 0.1504.$$

Interface 3: We will consider all three interlaminar stresses at this interface and compute the LHS of Equation 6.12 as:

$$\left(\frac{0.73}{42.75}\right)^2 + \left(\frac{9.91}{68.95}\right)^2 + \left(\frac{67.47}{68.95}\right)^2 = 0.9784.$$

Thus, according to Equation 6.12, only interface 1 is expected to fail by delamination at $N_{xx} = 410$ kN/m.

6.2 LAMINATE DESIGN CONSIDERATIONS

6.2.1 Design Philosophy

The design of a structure or a component is in general based on the philosophy of avoiding failure during a predetermined service life. However, what constitutes failure depends principally on the type of application involved. For example, the most common failure mode in a statically loaded structure made of a ductile metal is yielding beyond which a permanent deformation may occur in the structure. On the other hand, the design of the same structure in a fatigue load application must take into account the possibility of a brittle failure accompanied by negligible yielding and rapid crack propagation.

Unlike ductile metals, composite laminates containing fiber-reinforced thermoset polymers do not exhibit gross yielding, yet they are also not classic brittle materials. Under a static tensile load, many of these laminates show nonlinear characteristics attributed to sequential ply failures. The question that often arises in designing with such composite laminates is, "Should the design be based on the ultimate failure or the first ply failure?" The current design practice in the aircraft or aerospace industry uses the FPF approach, primarily since cracks appearing in the failed ply may make the neighboring plies susceptible to mechanical and environmental damage. In many laminated constructions, the ultimate failure occurs soon after the FPF (Table 6.4), and therefore with these laminates an FPF design approach is justified. For many other laminates, the difference between the FPF stress level and the ultimate strength level is quite high. An FPF design approach with these laminates may be considered somewhat conservative.

The behavior of a fiber-reinforced composite laminate in a fatigue load application is also quite different from that of metals. In a metal, nearly 80%–90% of its fatigue life is spent in the formation of a critical crack. Generally, the fatigue crack in a metal is not detectable by the present-day NDT techniques until it reaches the critical length. However, once the fatigue crack attains the critical length, it propagates rapidly through the structure, failing it in a catastrophic manner (Figure 6.7). In many polymer matrix composites, fatigue damage may appear at multiple locations in the first few hundred to a thousand cycles. Some of these damages, such as surface craze marks, fiber splitting, and edge delaminations, may also be visible in the early stages of the fatigue life. Unlike metals, the propagation or further accumulation of damage in a fiber-reinforced composite takes place in a progressive manner resulting in a gradual loss in the stiffness of the structure. Thus, the laminated composite structure continues to carry the load without failing catastrophically; however, the loss of its stiffness may create gradually increasing deflections or vibrations. In these situations, a fatigue design approach based on the appearance of the first mechanical damage may again be considered conservative.

Since the history of their development is new, very few long-term field performance experiences exist. Design data in the areas of combined stresses, cumulative fatigue, repeated impact, environmental damage, and so on are not available. There is very little agreement among designers about what constitutes a structural failure and how to predict it. Industry-wide standards for material specifications, quality control, test methods, and failure analysis have not yet been developed. For all these reasons, the development of fiber-reinforced composite parts often relies on empirical approaches and requires extensive prototyping and testing.

6.2.2 Design Criteria

In general, the current design practice for fiber-reinforced composite structures uses the same design criteria as those used for metals. For example, the primary

TABLE 6.4
Predicted Tensile Properties of $[0_2/\pm45]_S$ and $[0/90]_S$ Laminates

		First Ply Failure (FPF)			Ultimate Failure		
Material	Laminate	Stress, MPa (ksi)	Strain (%)	Modulus, GPa (Msi)	Stress, MPa (ksi)	Strain (%)	Modulus, GPa (Msi)
S-glass–epoxy	$[0_2/\pm45]_S$	345.5 (50.1)	1.34	25.5 (3.7)	618.0 (89.6)	2.75	19.3 (2.8)
	$[0/90]_S$	89.7 (13.0)	0.38	23.4 (3.4)	547.6 (79.4)	2.75	19.3 (2.8)
HTS carbon–epoxy	$[0_2/\pm45]_S$	591.1 (85.7)	0.72	82.1 (11.9)	600.0 (87.0)	0.83	82.8 (12.0)
	$[0/90]_S$	353.1 (51.2)	0.45	78.6 (11.4)	549.0 (79.6)	0.72	72.4 (10.5)

Source: Adapted from Halpin, J.C., *J. Compos. Mater.*, 6, 208, 1972.

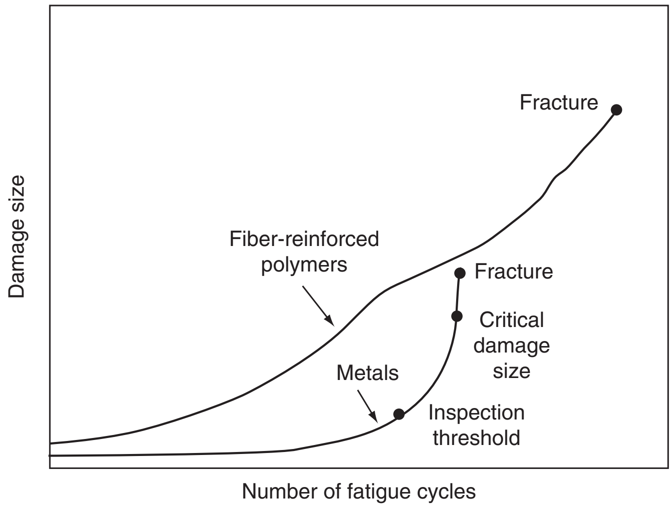

FIGURE 6.7 Schematic representation of damage development in metals and fiber-reinforced polymers. (Adapted from Salkind, M.J., *Composite Materials: Testing and Design* (*2nd Conference*), *ASTM STP*, 497, 143, 1972.)

structural components in an aircraft, whether made from an aluminum alloy or a carbon fiber-reinforced epoxy, are designed on the basis of the following criteria.

1. They must sustain the design ultimate load (DUL) in static testing.
2. The fatigue life must equal or exceed the projected vehicle life.
3. Deformations resulting from the applications of repeated loads and limit design load must not interfere with the mechanical operation of the aircraft, adversely affect its aerodynamic characteristics, or require repair or replacement of parts.

The DUL consists of the design limit load (DLL) multiplied by a specified ultimate factor of safety. The DLL is the maximum load that the structure (or any of its parts) is likely to experience during its design life. At the DLL, the structure should not undergo any permanent deformation. For metallic components, the most commonly used factor of safety is 1.5, although in fatigue-critical components it may be raised to 1.95. A higher factor of safety, such as 2 or more, is often used with fiber-reinforced composite materials, principally owing to the lack of design and field experience with these materials.

6.2.3 Design Allowables

Design allowable properties of a composite laminate are established by two different methods, namely, either by testing the laminate itself or by using the lamination theory along with a ply-level material property database. Considering the wide variety of lamination possibilities with a given fiber–resin combination, the second method is preferred by many designers since it has the flexibility of creating new design allowables without recourse to extensive testing.

The ply-level database is generated by testing unnotched unidirectional specimens in the tension, compression, and shear modes. The basic characteristics of the lamina, such as its longitudinal, transverse, and shear moduli, Poisson's ratios, and longitudinal, transverse, and shear strengths, as well as strains-to-failure, are determined by the various static test procedures described in Chapter 4. These tests are usually performed at room temperature; however, the actual application environment should also be included in the test program. The lamination theory combined with a failure criterion and a definition of failure is then used to predict the design allowables for the selected lamination configuration. This approach is particularly advantageous in generating design charts (also called carpet plots) for a family of laminates with the same basic ply orientations. Two of these charts for the $[0/\pm45/90]_S$ family of a carbon fiber–epoxy composite are shown in Figures 6.8 and 6.9. Such charts are very useful in selecting the proportions of the various ply orientations required to meet the particular design criteria involved [20].

Owing to the statistical nature of the ultimate properties, the design allowable strengths and strains are usually presented on one of the following bases:

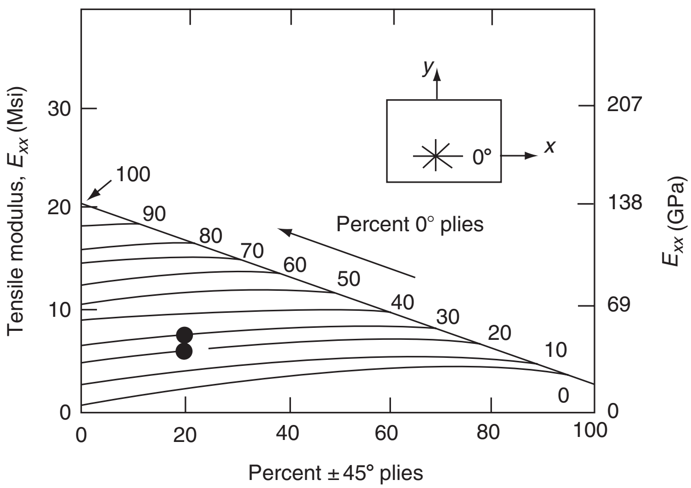

FIGURE 6.8 Carpet plot for tensile modulus E_{xx} of a carbon fiber–epoxy $[0/90/\pm45]_S$ laminate family. Note that the percentage of 90° plies is equal to 100 − (percentage of 0° plies) − (percentage of ±45° plies).

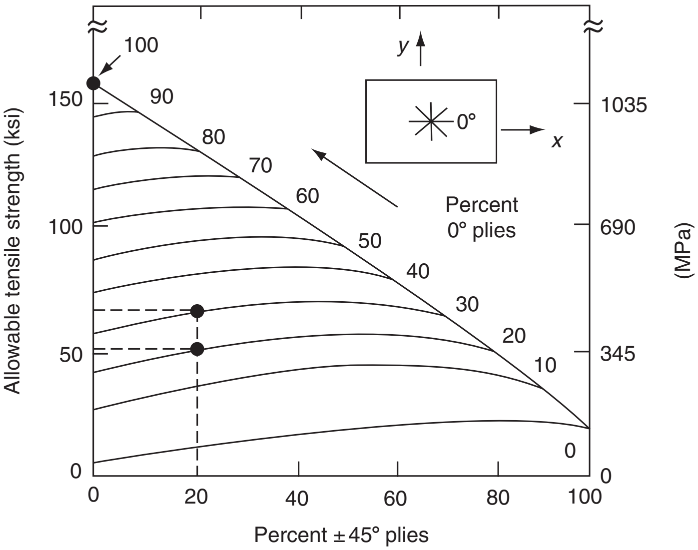

FIGURE 6.9 Carpet plot for tensile strength σ_{xx} of a carbon fiber–epoxy $[0/90/\pm45]_S$ laminate family.

1. *A basis*: Designed on the A-basis strength or strain, a component has at least a 99% probability of survival with a confidence level of 95%.
2. *B basis*: Designed on the B-basis strength or strain, a component has at least a 90% probability of survival with a confidence level of 95%.

Statistical methods to generate A- and B-basis design allowables are briefly described in Appendix A.8. The B-basis design allowables are commonly used for fiber-reinforced composite laminates, since the failure of one or more plies in these materials does not always result in the loss of structural integrity. Ekvall and Griffin [21] have described a step-by-step procedure of formulating the B-basis design allowables for T-300 carbon fiber–epoxy unidirectional and multidirectional laminates. Their approach also takes into account the effects of a 4.76 mm (0.1875 in.) diameter hole on the design allowable static strengths of these laminates.

In establishing the fatigue strength allowables for composite helicopter structures, Rich and Maass [22] used the mean fatigue strength minus 3 standard deviations. They observed that extrapolating the tension–tension fatigue data to the tension–compression or compression–compression mode may not be applicable for composite materials since significant fatigue strength reductions are possible in these two modes. Ply-level static and fatigue tests in their program were conducted under a room-temperature dry (RTD) as well as at an elevated-temperature wet (ETW) condition. The ETW condition selected was more severe than the actual design environment for helicopters. However, this

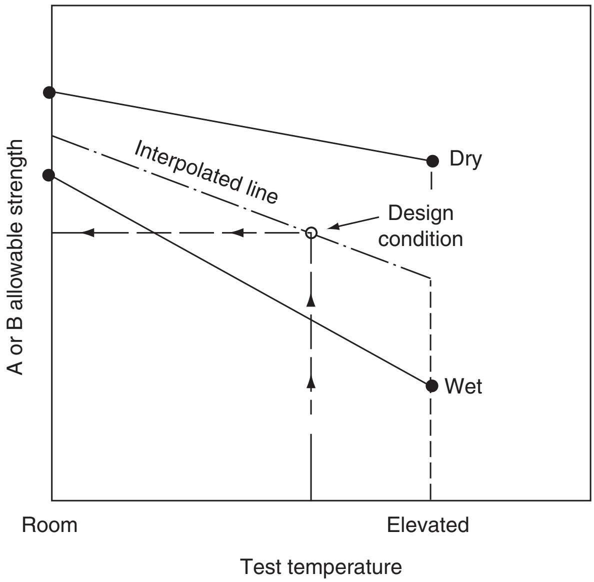

FIGURE 6.10 Linear interpolation method for determining design allowables.

procedure of testing at an ETW exceeding the design condition allows the designer to determine the allowable values for a variety of environmental conditions within the range investigated by interpolation rather than by extrapolation (Figure 6.10).

6.2.4 General Design Guidelines

The principal steps in designing a composite laminate are

1. Selection of fiber, resin, and fiber volume fraction
2. Selection of the optimum fiber orientation in each ply and the lamina stacking sequence
3. Selection of the number of plies needed in each orientation, which also determines the final thickness of the part

Considering these variables, it is obvious that a large variety of laminates may be created even if the ply orientations are restricted to a single family, such as a $[0/\pm45/90]_S$ family. Thus in most cases there is no straightforward method of designing a composite laminate unless the problem involves a simple structure, such as a rod or a column, and the loading is uniaxial.

From the standpoint of design as well as analytic simplicity, symmetric laminates are commonly preferred over unsymmetric laminates. This eliminates the extension–bending coupling represented by the $[B]$ matrix. The presence of extension–bending coupling is also undesirable from the stiffness standpoint, since it reduces the effective stiffness of the laminate and thereby increases its deflection, reduces the critical buckling loads, and decreases the natural frequency of vibration. Similar but lesser effects are observed if the laminate has bending–twisting coupling due to the presence of D_{16} and D_{26} terms. However, unless the fibers are at 0, 90, or 0/90 combinations, a symmetric laminate cannot be designed with $D_{16} = D_{26} = 0$.

The deleterious free-edge effects in a laminate can be reduced through proper selection of lamina stacking sequence. If angle-ply laminates are used, the layers with $+\theta$ and $-\theta$ orientations should be alternated instead of in a clustered configuration [23]. Thus, for example, an eight-layer laminate with four layers of $+\theta$ orientations and four layers of $-\theta$ orientations should be designed as $[+\theta/-\theta/+\theta/-\theta]_S$ instead of $[\theta/\theta/-\theta/-\theta]_S$ or $[-\theta/-\theta/+\theta/+\theta]_S$. However, if a laminate contains 0, 90, and $\pm\theta$ layers, adjacent $+\theta$ and $-\theta$ layers should be avoided. For example, in the quasi-isotropic laminate family containing 0, 90, and ± 45 layers, a $[45/0/90/-45]_S$ configuration is preferred over a $[90/+45/-45/0]_S$ or a $[0/+45/-45/90]_S$ configuration.

6.2.4.1 Laminate Design for Strength

When the state of stress in a structure is known and does not change during the course of its service operation, the lamina orientations may be selected in the following way [24].

Using the standard Mohr's circle technique, determine the principal normal loads and the principal directions. Analytically, the principal normal loads are

$$N_1 = \frac{1}{2}(N_{xx} + N_{yy}) + \left[\left(\frac{N_{xx} - N_{yy}}{2}\right)^2 + N_{xy}^2\right]^{1/2},$$

$$N_2 = \frac{1}{2}(N_{xx} + N_{yy}) - \left[\left(\frac{N_{xx} - N_{yy}}{2}\right)^2 + N_{xy}^2\right]^{1/2}, \tag{6.13}$$

and the principal direction with respect to the x axis is

$$\tan 2\theta = \frac{2N_{xy}}{N_{xx} - N_{yy}}. \tag{6.14}$$

Select a $[0_i/90_j]_S$ cross-ply configuration with the 0° layers aligned in the direction of the maximum principal load N_1 and the 90° layers aligned in the direction of the minimum principal load N_2. Thus with respect to the x axis, the laminate configuration is $[\theta_i/(90+\theta)_j]_S$. The ratio of 0° to 90° plies, i/j, is equal to the principal load ratio N_1/N_2.

When the stress state in a structure varies in direction or is unknown, a common approach in laminate design is to make it quasi-isotropic, for example,

$[0_i/\pm 45_j/90_k]_S$. The design procedure is then reduced to the selection of ply ratios ($i/j/k$) and the total thickness of the laminate. Design charts or carpet plots of the types shown in Figures 6.8 and 6.9 can be used to select the initial ply ratios; however, the final design must include a ply-by-ply analysis of the entire laminate.

Massard [25] has used an iterative ply-by-ply approach for designing symmetric laminates under in-plane and bending loads. In this approach, an initial laminate configuration is assumed and additional plies are added in a stepwise fashion to achieve the most efficient laminate that can sustain the given loading condition. At each step, strains in each lamina and the margin of safety (ratio of lamina strength to effective lamina stress) for each lamina are calculated. A margin of safety greater than unity indicates a safe ply in the laminate. The process is repeated until the margin of safety in each lamina is greater than unity.

Park [26] has used a simple optimization procedure to determine the fiber orientation angle θ for maximum FPF stress in symmetric laminates, such as $[\pm\theta]_S$, $[-\theta/0/\theta]_S$, and so on. The objective function F was expressed as

$$F = \varepsilon_{xx}^{\circ 2} + \varepsilon_{yy}^{\circ 2} + \frac{1}{2}\gamma_{xy}^{\circ 2}. \tag{6.15}$$

For a given laminate configuration, the midplane strain components are functions of the applied in-plane loads (N_{xx}, N_{yy}, and N_{xy}) as well as the fiber orientation angle θ. If the in-plane loads are specified, the design optimization procedure reduces to finding θ for which the objective function is minimum.

EXAMPLE 6.8

Using the carpet plots in Figures 6.8 and 6.9, determine the number of layers of 0, 90, and ±45° orientations in a quasi-isotropic $[0/90/\pm 45]_S$ laminate that meets the following criteria:

1. Minimum modulus in the axial (0°) direction $= 6 \times 10^6$ psi
2. Minimum B-allowable strength in the axial (0°) direction $=$ 65 ksi

Solution

Step 1: Referring to Figure 6.8, determine the ply ratio that gives $E_{xx} = 6 \times 10^6$ psi.

$$0{:}90{:}\pm 45 = 20\%{:}\,60\%{:}\,20\%$$

Step 2: Referring to Figure 6.9, check the B-allowable strength for the ply ratio determined in Step 1, which in our case is 51 ksi. Since this value is less than the minimum required, we select a new ply ratio that will give a minimum B-allowable strength of 65 ksi. This new ply ratio is 0:90:±45 $=$ 30:50:20. Referring back to Figure 6.8, we find that this ply ratio gives an axial modulus of 7×10^6 psi, which is higher than the minimum required in the present design. Thus, the laminate configuration selected is $[0_3/90_5/\pm 45_2]_S$.

Step 3: Assuming that the ply thickness is 0.005 in., we determine the ply thickness for each fiber orientation as

$$0^\circ: 6 \times 0.005 \text{ in.} = 0.03 \text{ in.}$$
$$90^\circ: 10 \times 0.005 \text{ in.} = 0.05 \text{ in.}$$
$$+45^\circ: 4 \times 0.005 \text{ in.} = 0.02 \text{ in.}$$
$$-45^\circ: 4 \times 0.005 \text{ in.} = 0.02 \text{ in.}$$

Thus, the total laminate thickness is 0.12 in.

6.2.4.2 Laminate Design for Stiffness

The stiffness of a member is a measure of its resistance to deformation or deflection owing to applied loads. If the member is made of an isotropic material, its stiffnesses are given by

$$\begin{aligned} \text{Axial stiffness} &= EA_0, \\ \text{Bending stiffness} &= EI_c, \\ \text{Torsional stiffness} &= GJ_c, \end{aligned} \tag{6.16}$$

where
E = modulus of elasticity
G = shear modulus
A_0 = cross-sectional area
I_c = moment of inertia of the cross section about the neutral axis
J_c = polar moment of inertia of the cross section

The stiffness equations for composite members are in general more involved than those given in Equation 6.16. If the composite member is made of a symmetric laminate, its stiffness against the in-plane loads is related to the elements in the [A] matrix, whereas its stiffness against bending, buckling, and torsional loads is related to the elements in the [D] matrix. The elements in both [A] and [D] matrices are functions of the fiber type, fiber volume fraction, fiber orientation angles, lamina thicknesses, and the number of layers of each orientation. In addition, the elements in the [D] matrix depend strongly on the lamina stacking sequence.

Except for 0, 90, and 0/90 combinations, the [D] matrix for all symmetric laminates contains nonzero D_{16} and D_{26} terms. Closed-form solutions for bending deflections, buckling loads, and vibrational frequencies of general symmetric laminates are not available. The following closed-form solutions [27,28] are valid for the special class of laminates for which $D_{16} = D_{26} = 0$ and the elements in the [B] matrix are negligible:

1. Center deflection of a simply supported rectangular plate carrying a uniformly distributed load p_0:

$$w \cong \frac{16p_0R^4b^4}{\pi^6}\left[\frac{1}{D_{11}+2(D_{12}+2D_{66})R^2+D_{22}R^4}\right] \tag{6.17}$$

2. Critical buckling load for a rectangular plate with pinned edges at the ends of its long dimension:

$$N_{\mathrm{cr}} \cong \frac{\pi^2[D_{11}+2(D_{12}+2D_{66})R^2+D_{22}R^4]}{b^2R^2} \tag{6.18}$$

3. Fundamental frequency of vibration for a simply supported rectangular plate:

$$f^2 \cong \frac{\pi^4}{\rho R^4b^4}[D_{11}+2(D_{12}+2D_{66})R^2+D_{22}R^4] \tag{6.19}$$

where

a = plate length
b = plate width
R = plate aspect ratio = a/b
ρ = density of the plate material

A few closed-form solutions are also available in the literature for unsymmetric laminates with a nonzero [B] matrix [27,28]. However, it has been shown that the coupling effect of the [B] matrix becomes small when the laminate contains more than six to eight layers [29]. Therefore, for most practical laminates, Equations 6.17 through 6.19 can be used for initial design purposes.

6.2.5 Finite Element Analysis

Design analysis of a laminated composite structure almost invariably requires the use of computers to calculate stresses and strains in each ply and to investigate whether the structure is "safe." For simple structures, such as a plate or a beam, the design analysis can be performed relatively easily. If the structure and the loading are complex, it may be necessary to perform the design analysis using finite element analysis. Commercially available finite element softwares, such as MSC-NASTRAN, ANSYS, ABAQUS, and LS-DYNA, have the capability of combining the lamination theory with the finite element codes. Many of these packages are capable of calculating in-plane as well as interlaminar stresses, incorporate more than one failure criterion, and contain a library of plate, shell, or solid elements with orthotropic material properties [30].

Although finite element analyses for both isotropic materials and laminated composite materials follow the same procedure, the problem of preparing the input data and interpreting the output data for composite structures is much more complex than in the case of metallic structures. Typical input information for an isotropic element includes its modulus, Poisson's ratio, and thickness. Its properties are assumed invariant in the thickness direction. An element for a composite structure may contain the entire stack of laminas. Consequently, in this case, the element specification must include the fiber orientation angle in each lamina, lamina thicknesses, and the location of each lamina with respect to the element midplane. Furthermore, the basic material property data for plane stress analysis of thin fiber-reinforced composite structure include four elastic constants, namely, the longitudinal modulus, transverse modulus, major Poisson's ratio, and shear modulus. Thus, the amount of input information even for a static load analysis of a composite structure is quite large compared with a similar analysis of a metallic structure.

The stress output from the finite element analysis of an isotropic material includes only three stress components for each element. In contrast, the stress output for a composite structure can be very large since it contains three in-plane stresses in each individual lamina as well as the interlaminar stresses between various laminas for every element. The lamina in-plane stresses are usually computed in the material principal directions, which vary from layer to layer within the same element. To examine the occurrence of failure in an element, a preselected failure criterion is applied to each lamina. In many finite element packages, the stress output may be reduced by calculating stress resultants, which are integrals of the lamina stresses through the thickness. However, interpretation of these stress resultants is difficult since they do not provide information regarding the adequacy of a design.

6.3 JOINT DESIGN

The purpose of a joint is to transfer loads from one member to another in a structure. The design of joints has a special significance in fiber-reinforced composite structures for two reasons: (1) the joints are often the weakest areas in a composite structure and (2) the composite materials do not possess the forgiving characteristics of ductile metals, namely, their capacity to redistribute local high stresses by yielding.

For composite laminates, the basic joints are either mechanical or bonded. Mechanical joints are created by fastening the substrates with bolts or rivets; bonded joints use an adhesive interlayer between the substrates (commonly called the adherends). The advantages and disadvantages of these two types of joints are listed as follows.

Mechanical Joints:

1. Permit quick and repeated disassembly for repairs or replacements without destroying the substrates
2. Require little or no surface preparation

3. Are easy to inspect for joint quality
4. Require machining of holes that interrupt the fiber continuity and may reduce the strength of the substrate laminates
5. Create highly localized stress concentrations around the joints that may induce failure in the substrates
6. Add weight to the structure
7. May create a potential corrosion problem, for example, in an aluminum fastener if used for joining carbon fiber–epoxy laminates

Bonded Joints:

1. Distribute the load over a larger area than mechanical joints
2. Require no holes, but may need surface preparation (cleaning, pretreatment, etc.)
3. Add very little weight to the structure
4. Are difficult to disassemble without either destroying or damaging substrates
5. May be affected by service temperature, humidity, and other environmental conditions
6. Are difficult to inspect for joint quality

We will now discuss the general design considerations with these two types of joints.

6.3.1 Mechanical Joints

The strength of mechanical joints depends on the following.

1. Geometric parameters, such as the ratios of edge distance to bolt hole diameter (e/d), width to bolt hole diameter (w/d), and laminate thickness to bolt hole diameter (h/d). In multibolt joints, spacing between holes and their arrangements are also important.
2. Material parameters, such as fiber orientation and laminate stacking sequence. Some of these material parameters are discussed in Chapter 4 (see Section 4.4.1).

In applications involving mechanical joints, three basic failure modes are observed in the substrates, namely, shear-out, net tension, and bearing failure (Figure 6.11). If the laminate contains nearly all 0° fibers, cleavage failure is also possible. From a safe design standpoint, a bearing failure is more desirable than either a shear-out or a net tension failure. However, unless the e/d and w/d ratios are very large, the full bearing strength is seldom achieved. In general, shear-out and net tension failures are avoided if $e/d > 3$ and $w/d > 6$. The actual geometric parameters are usually determined by conducting pin-bearing tests on the specific laminates involved. However, a bolted joint

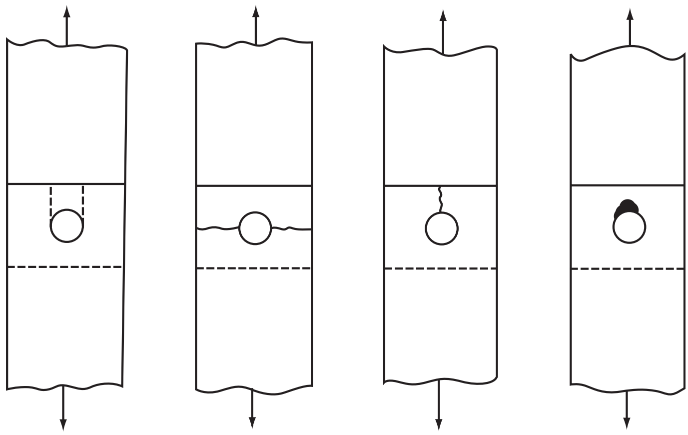

FIGURE 6.11 Basic failure modes in bolted laminates: (a) shear-out, (b) net tension failure, (c) cleavage, and (d) bearing failure. Combinations of these failure modes are possible.

differs from a pinned joint, since in the former the clamping torque is an added factor contributing to the joint strength. The edge distance needed to reduce shear-out failure can be reduced by increasing the laminate thickness at the edge or by inserting metal shims between various composite layers near the bolted area.

The strength of a mechanical joint can be improved significantly by relieving the stress concentrations surrounding the joint. The following are some of the methods used for relieving stress concentrations.

Softening strips of lower modulus material are used in the bolt bearing area. For example, strips made of E-glass fiber plies can be used to replace some of the carbon fiber plies aligned with the loading direction in a carbon fiber-reinforced laminate.

Laminate tailoring method [31] divides the bolt hole area of structure into two regions, namely, a primary region and a bearing region. This is demonstrated in Figure 6.12 for a structure made of a $[0_2/\pm 45]_{2S}$ laminate. In the bearing region surrounding the bolt hole, the 0° plies in the laminate are replaced by ±45° plies. Thus, the lower modulus bearing region is bounded on both sides by the primary region of $[0_2/\pm 45]$ laminate containing 20%–60% 0° plies. The majority of the axial load in the joint is carried by the high-modulus primary region, which is free of fastener holes. The combination of low axial stress in the bearing region and the relatively low notch sensitivity of the [±45] laminate delays the onset of the net tension failure commonly observed in non-tailored $[0_2/\pm 45]_S$ laminates.

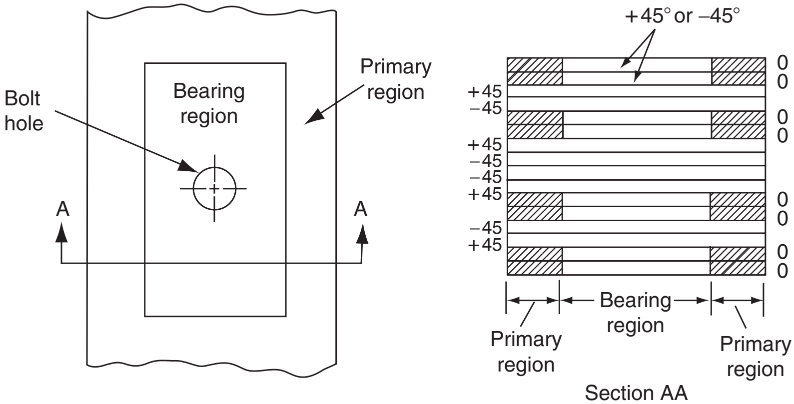

FIGURE 6.12 Laminate tailoring method for improving bolted joint strength.

Interference fit fasteners increase the possibility of localized delamination instead of fiber failure in the joint area (Figure 6.13). This leads to a redistribution of high stresses surrounding the joint. However, care must be taken not to damage the fibers while installing the interference fit fasteners.

Holes for mechanical joints can either be machined in a postmolding operation or formed during the molding of the part. Machining is preferred, since molded

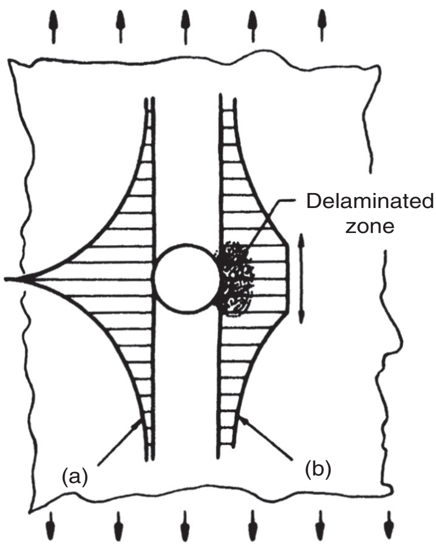

FIGURE 6.13 Stress distributions in areas adjacent to a bolt hole with (a) no delaminated zone and (b) a delaminated zone. (After Jones, R.M., Morgan, H.S., and Whitney, J.M., *J. Appl. Mech.*, 40, 1143, 1973.)

holes may be surrounded by misoriented fibers, resin-rich areas, or knit lines. Drilling is the most common method of machining holes in a cured laminate; however, unless proper cutting speed, sharp tools, and fixturing are used, the material around the drilled hole (particularly at the exit side of the drill) may be damaged. High-speed water jets or lasers produce cleaner holes and little or no damage compared with the common drilling process.

6.3.2 Bonded Joints

The simplest and most widely used bonded joint is a single-lap joint (Figure 6.14a) in which the load transfer between the substrates takes place through a distribution of shear stresses in the adhesive. However, since the loads applied at the substrates are off-centered, the bending action sets up a normal (peel) stress in the thickness direction of the adhesive. Both shear and normal stress distributions exhibit high values at the lap ends of the adhesive layer, which tends to reduce the joint strength. The double-lap joint, shown in Figure 6.14b, eliminates much of the bending and normal stresses present in the single-lap joint. Since the average shear stress in the adhesive is also reduced by nearly one-half, a double-lap joint has a higher joint strength than a single-lap joint (Figure 6.15). The use of a long-bonded strap on either side or on each side of the substrates (Figure 6.14c) also improves the joint strength over that of single-lap joints.

Stepped lap (Figure 6.14d) and scarf joints (Figure 6.14e) can potentially achieve very high joint strengths, however in practice, the difficulty in machining the steps or steep scarf angles often overshadows their advantages. If a

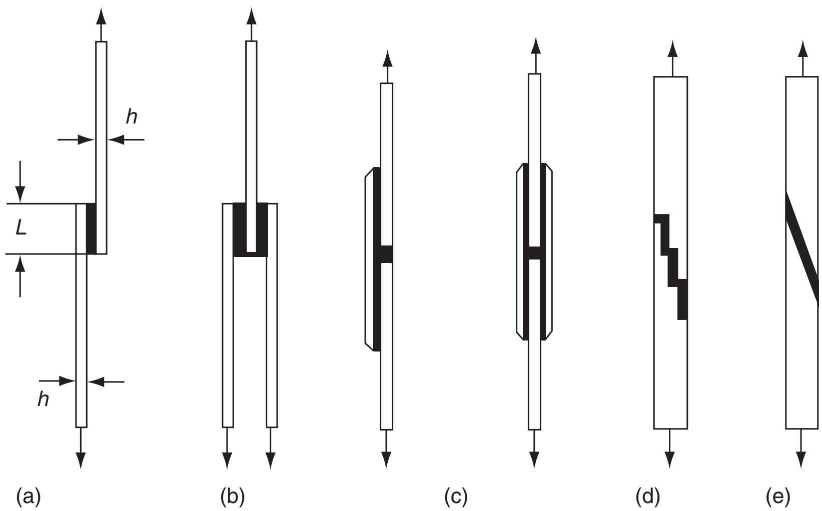

FIGURE 6.14 Basic bonded joint configurations: (a) single-lap joint, (b) double-lap joint, (c) single- and double-strap joints, (d) stepped lap joint, and (e) scarf joint.

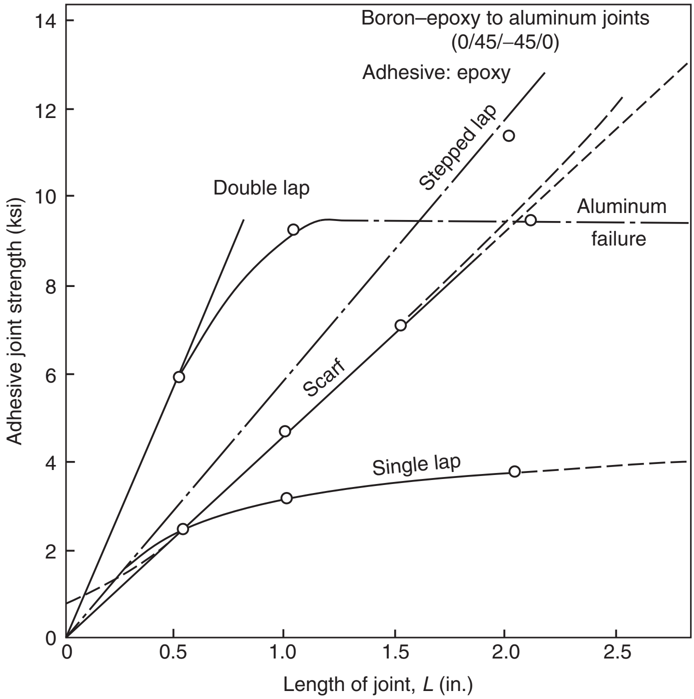

FIGURE 6.15 Increase in the joint strength of single-lap bonded joints with lap length. (After Griffin, O.H., *Compos. Technol. Rev.*, 4, 136, 1982.)

stepped lap joint is used, it may often be easier and less expensive to lay up the steps before cure. This eliminates the machining operation and prevents damage to the fibers.

The following points are important in designing a bonded joint and selecting an appropriate adhesive for the joint.

1. Increasing the ratio of lap length to substrate thickness h improves the joint strength significantly at small L/h ratios. At high L/h ratios, the improvement is marginal (Figure 6.16).
2. Tapering the substrate ends at the ends of the overlap reduces the high normal stresses at these locations [32].
3. Equal axial stiffnesses for the substrates are highly desirable for achieving the maximum joint strength (Figure 6.16). Since stiffness is a product of modulus E and thickness h, it is important to select the proper thickness of each substrate so that $E_1h_1 = E_2h_2$. If the two substrates are of the same material, their thicknesses must be equal.
4. The important characteristics of a good adhesive are high shear and tensile strengths but low shear and tensile moduli. An efficient way of

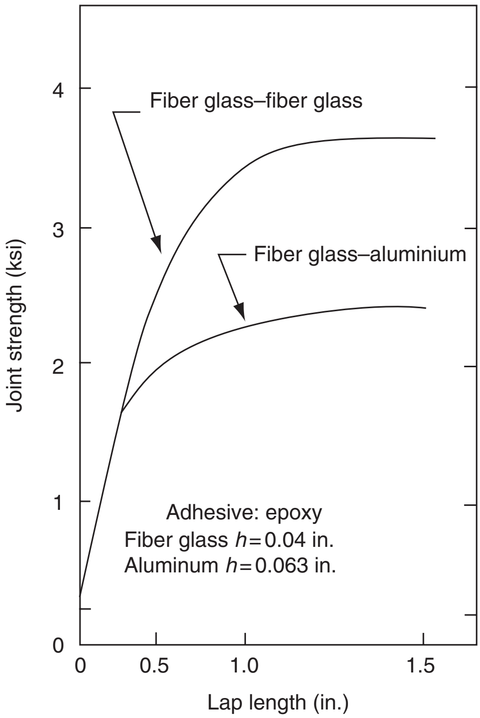

FIGURE 6.16 Comparison of joint strengths of various bonded joint configurations. (After Griffin, O.H., *Compos. Technol. Rev.*, 4, 136, 1982.)

increasing the joint strength is to use a low-modulus adhesive only near the ends of the overlap, which reduces stress concentrations, and a higher modulus adhesive in the central region, which carries a large share of the load. High ductility for the adhesive becomes an important selection criterion if the substrates are of dissimilar stiffnesses or if the joint is subjected to impact loads.

5. Fiber orientation in the laminate surface layers adjacent to the lap joints should be parallel to the loading direction (Figure 6.17). Otherwise, a scarf joint should be considered even though machining is required to produce this configuration.

6.4 DESIGN EXAMPLES

6.4.1 Design of a Tension Member

The simplest and the most efficient structure to design with a fiber-reinforced composite material is a two-force tension member, such as a slender rod or a slender bar subjected to tensile forces along its axis. Since the fibers have

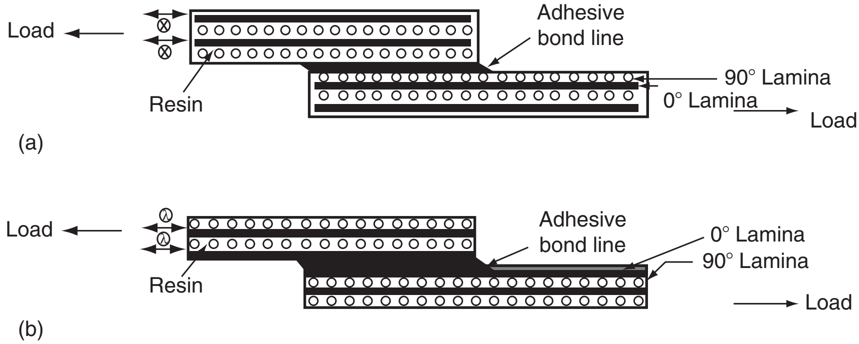

FIGURE 6.17 Examples of (a) poor and (b) good laminate designs for bonded joints. (After Ref. Griffin, O.H., *Compos. Technol. Rev.*, 4, 136, 1982.)

exceptionally high tensile strength–weight ratios, the load-carrying capacity of a tension member with fibers oriented parallel to its axis can be very high. The static tension load that can be supported by a tension member containing longitudinal continuous fibers is

$$P = S_{\mathrm{Lt}} A_0 \cong \sigma_{\mathrm{fu}} \mathrm{v_f} A_0, \tag{6.20}$$

where

σ_{fu} = ultimate tensile strength of the fibers
$\mathrm{v_f}$ = fiber volume fraction
A_0 = cross-sectional area

The axial stiffness of the tension member is

$$EA_0 \cong E_{\mathrm{f}} \mathrm{v_f} A_0, \tag{6.21}$$

so that its axial elongation can be written as

$$\Delta = \frac{PL_0}{EA_0} = \frac{\sigma_{\mathrm{fu}}}{E_{\mathrm{f}}} L_0. \tag{6.22}$$

Equations 6.20 and 6.21 indicate the importance of selecting the proper fiber type as well as the fiber volume fraction for maximum load-carrying capacity and stiffness of a tension member. For good fiber wet-out, the practical limit for the maximum fiber volume fraction is about 0.6. Thus, for a specified design load, the minimum cross-sectional area is obtained by selecting the strongest fiber. In many applications, however, the maximum elongation may also be specified. In that case, the ratio of fiber strength to fiber modulus should also be checked. Although selection of the matrix has little influence on the load-carrying capacity or the elongation, it can influence the manufacturing and environmental considerations for the member.

TABLE 6.5
Tensile Fatigue Strength Coefficient *b* for Various 0° Laminates

Fiber Type	*b*
Ultrahigh-modulus carbon	0.021
High-modulus carbon	0.035
High-strength carbon	0.05
Kevlar 49	0.035
S-glass	0.088
E-glass	0.093

For most 0° continuous fiber composites, the fatigue strength in tension–tension cycling can be approximated as

$$S = S_{\mathrm{Lt}}(1 - b \log N), \tag{6.23}$$

where the value of the constant b depends primarily on the fiber type (Table 6.5). If the tension member is exposed to tension–tension fatigue, its design should be based on the fatigue strength of the material at the desired number of cycles. It should be noted that ranking of the fibers based on the fatigue strength can be different from that based on the fiber tensile strength.

The most critical design issue for a tension member involves the joints or connections at its ends. A few joint design ideas other than the simple bolted or bonded joints are shown in Figure 6.18.

6.4.2 Design of a Compression Member

Tubular compression members made from fiber-reinforced polymeric materials are finding applications in many aerospace structures, such as satellite trusses, support struts, and flight control rods. Since these compression members are mostly slender tubes, their design is usually based on preventing overall column buckling as well as local buckling [33].

The compressive stress on a thin tube of radius r and wall thickness t is

$$\sigma = \frac{P}{A_0} = \frac{P}{2\pi r t}, \tag{6.24}$$

where P is the axial compressive load.

For a pin-ended column, the overall buckling stress is given by

$$\sigma_{\mathrm{col}} = \left(\frac{2L^2}{\pi^2 E_{xx} r^2} + \frac{2}{G_{xy}}\right)^{-1}, \tag{6.25}$$

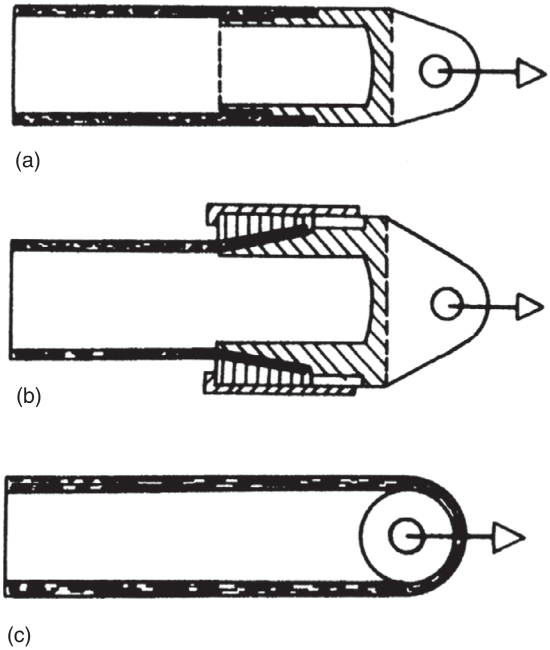

FIGURE 6.18 Joints in tension members: (a) tube with bonded shear fitting, (b) tube with wedge fitting, and (c) wrapping around a bushing. (Adapted from Taig, I.C., *Composites—Standards, Testing and Design*, National Physical Laboratory, London, 1974.)

where

L = length of the compression member
E_{xx} = modulus of elasticity in the axial direction
G_{xy} = shear modulus

Note that the second term in Equation 6.25 represents the shear effect on the critical buckling stress.

The local buckling stress of a thin-walled tube is given by

$$\sigma_{\text{local}} = \beta_0 \frac{t}{r}, \tag{6.26}$$

where

$$\beta_0 = \frac{\gamma \Phi \sqrt{E_{xx} E_{yy}}}{\sqrt{3(1 - \nu_{xy}\nu_{yx})}}$$

γ = a correlation coefficient

$$\Phi = \left[\frac{2G_{xy}}{\sqrt{E_{xx}E_{yy}}} (1 + \nu_{xy}\nu_{yx}) \right]^{1/2} \quad \text{or 1, whichever is smaller}$$

Using Equations 6.24 through 6.26, Maass [33] developed the following optimum stress equation for a compression tube design:

$$\sigma_{\text{opt}}^3\left[\frac{4}{\pi E_{xx}\beta_0(P/L^2)}\right]+\sigma_{\text{opt}}\left(\frac{2}{G_{xy}}\right)=1. \tag{6.27}$$

Neglecting the shear term, an approximate σ_{opt} can be calculated as

$$\sigma_{\text{opt}}=\left[\frac{\pi E_{xx}\beta_0(P/L^2)}{4}\right]^{1/3}, \tag{6.28}$$

where (P/L^2) is called the loading index.

Knowing σ_{opt} from either Equation 6.27 or 6.28, the actual tube dimensions can be determined from the following equations:

$$r_{\text{opt}}=\left(\frac{P\beta_0}{2\pi\sigma_{\text{opt}}^2}\right)^{1/2},$$

$$t_{\text{opt}}=\frac{\sigma_{\text{opt}}}{\beta_0}r_{\text{opt}}. \tag{6.29}$$

Equations 6.27 through 6.29 show that the optimum design of a compression tube depends very much on the laminate configuration. Maass [33] used these equations to determine the optimum stress and the corresponding ply ratio for various $[0/\pm\theta]_S$ tubes made of high-strength carbon–epoxy laminates. For a unit loading index, the highest optimum stress occurs for a $[0_3/\pm45]_S$ tube, although a $[\pm15]_S$ tube with no 0° fibers exhibits approximately the same optimum stress. The optimum design with increasing off-axis angle θ is obtained with increasing percentages of 0° layers in the tube.

6.4.3 Design of a Beam

Beams are slender structural members designed principally to resist transverse loads. In general, the stress state at any point in the beam consists of an axial normal stress σ_{xx} and a transverse shear stress τ_{xz}. Both these stresses are nonuniformly distributed across the thickness (depth) of the beam. In an isotropic homogeneous beam, these stress distributions are continuous with the maximum and minimum normal stresses occurring at the outermost surfaces and the maximum shear stress occurring at the neutral axis. In laminated beams, the normal stress and shear stress distributions are not only nonuniform, but also they are discontinuous at the interfaces of dissimilar laminas. Depending on the lamination configuration, it is possible to create maximum normal stresses in the interior of the beam thickness and the maximum shear stress away from the midplane of the beam. For this reason, the actual stress distribution in a laminated composite beam should always be calculated using the lamination theory instead of the homogeneous beam theory.

Except all 0, all 90, and 0/90 combinations for which $D_{16} = D_{26} = 0$, there will be a bending–twisting coupling in all symmetric beams. This means that a bending moment will create not only bending deformations, but also tend to twist the beam. Whitney et al. [34] have shown that the deflection equation for a symmetric beam has the same form as that for a homogeneous beam, namely,

$$\frac{d^2 w}{dx^2} = \frac{b M_{xx}}{E_b I}, \tag{6.30}$$

where

w = beam deflection
b = beam width
M_{xx} = bending moment per unit width
I = moment of inertia of the cross section about the midplane
E_b = effective bending modulus of the beam

The effective bending modulus E_b is defined as

$$E_b = \frac{12}{h^3 D_{11}^*}, \tag{6.31}$$

where

h is the beam thickness
D_{11}^* is the first element in the inverse [D] matrix (see Example 3.13)

Equation 6.31 neglects the effect due to transverse shear, which can be significant for beams with small span-to-thickness ratio. For long beams, for which the effect of the transverse shear is negligible, the maximum deflection can be calculated by replacing the isotropic modulus E with the effective bending modulus E_b in the deflection formulas for homogeneous beams. From Equation 6.31, the effective bending stiffness for a laminated beam can be written as

$$E_b I = \frac{b}{D_{11}^*}. \tag{6.32}$$

For a symmetric beam containing isotropic layers or specially orthotropic layers (such as all 0°, all 90°, or combinations of 0° and 90° layers), the effective bending stiffness becomes

$$(EI)_b = \Sigma (E_{11})_j I_j, \tag{6.33}$$

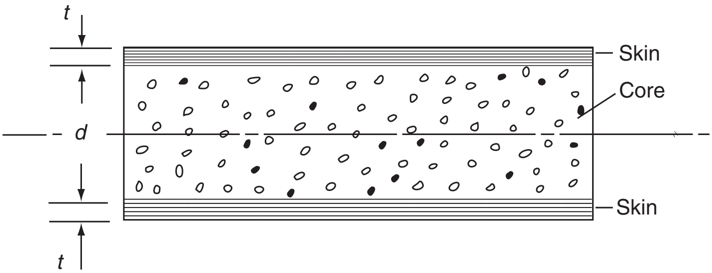

FIGURE 6.19 Construction of a sandwich beam.

where $(E_{11})_j$ is the longitudinal modulus of the jth layer and I_j is the moment of inertia of the jth layer with respect to the midplane

The most effective method of reducing the weight of a beam (or a panel) without sacrificing its bending stiffness is to use a sandwich construction (Figure 6.19). This consists of a lightweight, low-modulus foam or honeycomb core adhesively bonded to high-modulus fiber-reinforced laminate skins (face-sheets). The bending stiffness of the sandwich beam is

$$(EI)_\mathrm{b} = E_\mathrm{s}\frac{bt^3}{6} + 2bE_\mathrm{s}t\left(\frac{d+t}{2}\right)^2 + E_\mathrm{c}\frac{bd^3}{12}, \tag{6.34}$$

where

E_s = modulus of the skin material
E_c = modulus of the core material ($E_\mathrm{c} << E_\mathrm{s}$)
b = beam width
t = skin thickness
d = core thickness

Equation 6.34 shows that the bending stiffness of a sandwich beam can be increased significantly by increasing the value of d, that is, by using a thicker core. Since the core material has a relatively low density, increasing its thickness (within practical limits) does not add much weight to the beam. However, it should be noted that the core material also has a low shear modulus. Thus, unless the ratio of span to skin thickness of the sandwich beam is high, its deflection will be increased owing to the transverse shear effect.

Commonly used core materials are honeycombs with hexagonal cells made of either aluminum alloys or aramid fiber-reinforced phenolics.* The strength and stiffness of such cores depend on the cell size, cell wall thickness, and the material used in the honeycomb. High core strength is desirable to resist

* Trade name: Nomex, manufactured by Du Pont.

transverse shear stresses as well as to prevent crushing of the core under the applied load. While the facings in a sandwich beam or panel resist tensile and compressive stresses induced due to bending, the core is required to withstand transverse shear stresses, which are high near the center of the beam cross section. The core must also have high stiffness to resist not only the overall buckling of the sandwich structure but also local wrinkling of the facing material under high compressive loads.

Proper fiber selection is important in any beam design. Although beams containing ultrahigh-modulus carbon fibers offer the highest flexural stiffness, they are brittle and exhibit a catastrophic failure mode under impact conditions. The impact energy absorption of these beams can be increased significantly by using an interply hybrid system of ultrahigh-modulus carbon fibers in the skin and glass or Kevlar 49 fibers in the core. Even with lower modulus carbon fibers, hybridization is recommended since the cost of a hybrid beam is lower than an all-carbon beam. Beams containing only Kevlar 49 fibers are seldom used, since composites containing Kevlar 49 fibers have low compressive strengths. In some beam applications, as in the case of a spring, the capacity of the beam to store elastic strain energy is important. In selecting fibers for such applications, the elastic strain energy storage capacity of the fibers should be compared (Table 6.6).

EXAMPLE 6.9

Design of a Hybrid Beam. Determine the thickness of 25.4 mm (1 in.) wide hybrid beam containing three layers of HMS carbon–epoxy and two layers of S-glass–epoxy to replace a steel beam of bending stiffness 26.2 kN m^2 (150 lb in.^{2}). Fibers in the composite beam are parallel to the beam axis. Assuming that each carbon fiber ply is 0.15 mm (0.006 in.) thick and each glass fiber ply is 0.13 mm (0.005 in.) thick, determine the number of plies required for each fiber type.

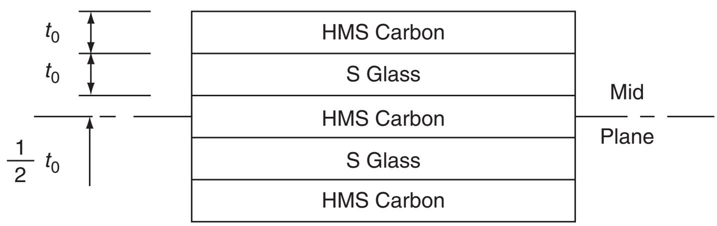

Solution

For maximum stiffness, we place two carbon fiber layers on the outside surfaces. For symmetry, the layers just below the outside carbon layers will be the S-glass layers, which will leave the remaining carbon fiber layer at the center of the cross section. We assume that each layer has a thickness t_0. Since fibers in each layer are

TABLE 6.6
Strain Energy Storage Capacity of E-Glass and Carbon Fiber Laminates

					Strain Energy Capacity[a]		
	Density, g/cm^3	Strength, MPa (ksi)		Modulus,	Per Unit Volume, kN m/m^3	Per Unit Weight, kN m/kg	Per Unit Cost,[b]
Material	(lb/in.^{3})	Static	Fatigue	GPa (Msi)	(lb in./in.^{3})	(lb in./lb)	kN m/$ (lb in./$)
Spring steel	7.84 (0.283)	1448 (210)	724 (105)	200 (29)	1310 (190)	167 (672)	253 (2240)
E-glass–epoxy	1.77 (0.064)	690 (100)	241 (35)	38 (5.5)	765 (111)	432 (1734)	245 (2167)
High-strength carbon–epoxy	1.50 (0.054)	1035 (150)	672 (97.5)	145 (21)	1558 (226)	1041 (4185)	23.6 (209)

[a] Strain energy per unit volume = strength^2/(2 × modulus). In this table, strain energy is calculated on the basis of fatigue strength.
[b] Cost: Steel = \$0.30/lb, E-glass–epoxy = \$0.80/lb, high-strength carbon–epoxy = \$20/lb.

at a 0° orientation with the beam axis, we can apply Equation 6.33 to calculate the bending stiffness of the hybrid beam. Thus,

$$
\begin{aligned}
(EI)_{\text{hybrid}} &= 2E_{\text{c}}I_1 + 2E_{\text{g}}I_2 + E_{\text{c}}I_3 \\
&= 2E_{\text{c}}\left[\frac{1}{12}bt_0^3 + bt_0\left(t_0 + \frac{1}{2}t_0 + \frac{1}{2}t_0\right)^2\right] \\
&\quad + 2E_{\text{g}}\left[\frac{1}{12}bt_0^3 + bt_0\left(\frac{1}{2}t_0 + \frac{1}{2}t_0\right)^2\right] + E_{\text{c}}\left[\frac{1}{12}bt_0^3\right] \\
&= \frac{1}{12}bt_0^3(99E_{\text{c}} + 26E_{\text{g}}).
\end{aligned}
$$

Substituting $E_{\text{c}} = 207$ GPa, $E_{\text{g}} = 43$ GPa (from Appendix A.5), and $b = 0.0254$ m into the equation for bending stiffness and equating it to 26.2 kN m^2, we calculate $t_0 = 8.3$ mm (0.33 in.). Since there are five layers, the total thickness of the beam is 41.5 mm (1.65 in.). In comparison, the thickness of the steel beam of the same width is 39 mm (1.535 in.).

Now we calculate the number of plies for each layer by dividing the layer thickness by the ply thickness. For HMS carbon fibers, the number of plies in each layer is 55.3, or 56, and that for the S-glass layers is 63.8, or 64.

6.4.4 Design of a Torsional Member

The shear modulus of many fiber-reinforced composites is lower than that for steel. Thus for an equivalent torsional stiffness, a fiber-reinforced composite tube must have either a larger diameter or a greater thickness than a steel tube. Among the various laminate configurations, $[\pm 45]_{\text{S}}$ laminates possess the highest shear modulus and are the primary laminate type used in purely torsional applications.

In general, the shear modulus of a laminate increases with increasing fiber modulus. Thus, for example, the shear modulus of a GY-70 carbon–epoxy $[\pm 45]_{\text{S}}$ laminate is 79.3 GPa (11.5 Msi), which is equivalent to that of steel. The shear modulus of an AS carbon–epoxy $[\pm 45]_{\text{S}}$ laminate is 31 GPa (4.49 Msi), which is slightly better than that of aluminum alloys. Glass fiber laminates have even lower shear modulus, and Kevlar 49 fiber laminates are not generally used in torsional applications because of their low shear strengths. The shear strengths of both GY-70 and AS carbon–epoxy $[\pm 45]_{\text{S}}$ laminates are comparable with or even slightly better than those for mild steel and aluminum alloys.

The maximum torsional shear stress in a thin-walled tube of balanced symmetric laminate constructions [35] is

$$
\tau_{xy} = \frac{T}{2\pi r^2 t} \tag{6.35}
$$

and the angle of twist per unit length of the tube is given by

$$\phi = \frac{T}{2\pi G_{xy} r^3 t}, \tag{6.36}$$

where
  T = applied torque
  r = mean radius
  t = wall thickness

For very thin-walled tubes, the possibility of torsional buckling exists. For symmetrically laminated tubes of moderate lengths, the critical buckling torque [36] is

$$T_{cr} = 24.4 C D_{22}^{5/8} A_{11}^{3/8} r^{5/4} L^{-1/2}, \tag{6.37}$$

where C is end-fixity coefficient, which is equal to 0.925 for simply supported ends and 1.03 for clamped ends.

EXAMPLE 6.10

Design of an Automotive Drive Shaft. Select a laminate configuration for an automotive drive shaft that meets the following design requirements:

1. Outer diameter = 95.25 mm (3.75 in.)
2. Length = 1.905 m (75 in.)
3. Minimum resonance frequency = 90 Hz
4. Operating torque = 2,822 N m (25,000 in. lb)
5. Overload torque = 3,386 N m (30,000 in. lb)

Use a carbon–epoxy laminate containing 60% by volume of T-300 carbon fibers. The ply thickness is 0.1524 mm (0.006 in.). The elastic properties of the material are given in Example 3.6. The static shear strength for a $[\pm 45]_S$ laminate of this material is 455 MPa (66,000 psi).

SOLUTION

Step 1: Select an initial laminate configuration, and determine the minimum wall thickness for the drive shaft.

The primary load on the drive shaft is a torsional moment for which we select a $[\pm 45]_{kS}$ laminate, where k stands for the number of $\pm 45°$ layers in the laminate. The minimum wall thickness for the laminate is determined from the following equation:

$$\tau_{all} = \frac{S_{xys}}{n} = \frac{T_{max}}{2\pi r^2 t},$$

where

$T_{\max}$ = maximum torque = 3386 N m
r = mean radius = 0.048 m
t = wall thickness
S_{xys} = static shear strength = 455×10^6 N/m^2
n = factor of safety = 2.2 (assumed)

Using this equation, we calculate $t = 0.001131$ m = 1.131 mm. Since each ply is 0.1524 mm thick, the minimum number of 45° plies is (1.131/0.1524) = 7.42. Assume eight plies, so that the initial laminate configuration is $[\pm 45]_{2S}$.

Step 2: Check for the minimum resonance frequency. The fundamental resonance frequency corresponding to the critical speed of a rotating shaft is

$$f_{cr} = \frac{1}{2\pi}\left[\frac{\pi^2}{L^2}\sqrt{\frac{E_{xx}I_c}{\rho A_0}}\right],$$

where

E_{xx} = axial modulus
A_0 = $2\pi r t$
I_c = $\pi r^3 t$
ρ = density

Substituting for A_0 and I_c, we obtain

$$f_{cr} = \frac{\pi}{2}\frac{r}{L^2}\sqrt{\frac{E_{xx}}{2\rho}}.$$

To meet the minimum resonance frequency, the shaft must have an adequate axial modulus. Since the axial modulus of a $[\pm 45]_{2S}$ laminate is rather low, we add four plies of 0° layers to the previous ±45° layers so that the new laminate configuration is $[\pm 45/0_2/\pm 45]_S$. The two 45° layers are placed in the outer diameter instead of the 0° layers to resist the maximum shear stress due to the torsional moment. Using the lamination theory, we calculate E_{xx} as 53.39 GPa. Since the ply material contains 60% by volume of T-300 carbon fibers, its density is calculated as 1556 kg/m^3. Using these values, we calculate the resonance frequency as 86 Hz, which is less than the minimum value required.

To improve the resonance frequency, we add two more layers of 0° plies, which brings the laminate configuration to $[\pm 45/0_3/\pm 45]_S$. Using the lamination theory, we recalculate E_{xx} as 65.10 GPa. The resonance frequency of this new shaft is 95 Hz, which exceeds the minimum value required.

Step 3: Check for the maximum torsional shear stress. We need to check for the maximum torsional shear stress since the laminate configuration is different from that assumed in Step 1. The $[\pm 45/0_3/\pm 45]_S$ laminate contains 14 plies with a wall thickness of 14×0.1524 mm = 2.13 mm. The maximum torsional shear stress is calculated as 109.8 MPa.

The maximum static shear strength of the $[\pm 45/0_3/\pm 45]_S$ laminate is not known. Since 57% of this laminate is ±45° layers, we estimate its shear strength as 57% of the static shear strength of the $[\pm 45]_S$ laminate, or 0.57×455 MPa $=$ 260 MPa. Comparing the maximum torsional shear stress with this estimated shear strength, we find the factor of safety as $n = 260/109.8 = 2.37$, which is adequate for the torsional shear stress.

Step 4: Check the critical buckling torque. Using the lamination theory, we calculate $D_{22} = 71.48$ N m and $A_{11} = 1714.59 \times 10^5$ N/m. Substitution of these values into Equation 6.37 gives $T_{cr} = 6420$ N m, which is nearly twice the maximum application torque. Thus the $[\pm 45/0_3/\pm 45]_S$ laminate is safe against torsional buckling. If this were not the case, the easiest way to increase the critical buckling torque would be to increase D_{22}, which is achieved by adding one or more 90° plies on both sides of the laminate midplane.

Although this example does not address the problem of the end fitting attachments, it is a critical design issue for an automotive drive shaft. The common methods of attaching the metal end fittings are bonded or interference joints for low applied torques and bonded or bolted joints for high applied torques. If bolting is used, it is recommended that the joint area be locally reinforced either by using a tubular metal insert or by using additional layers in the laminate.

6.5 APPLICATION EXAMPLES

6.5.1 Inboard Ailerons on Lockheed L-1011 Aircraft [37]

Ailerons are adjustable control surfaces hinged to the wing trailing edges of an aircraft for controlling its roll (rotation about the longitudinal axis). Their angular positions are manipulated by hydraulic actuators. Each aileron has a wedge-shaped one-cell box configuration consisting of a front spar, a rear spar, upper and lower covers, and a number of reinforcing ribs. Other parts in the aileron assembly are leading edge shrouds, end fairings, trailing edge wedge, shroud supports, feedback fittings, and hinge and actuator fittings. The primary load on the aileron surfaces is the air pressure. Ailerons are not considered primary structural components in an aircraft. Like other secondary components, their design is governed by stiffness instead of strength.

In Lockheed L-1011 aircraft, inboard ailerons are located between the outboard and inboard flaps on each wing (Figure 6.20). At the front spar, each aileron is 2.34 m (92 in.) in length and ~250 mm (10 in.) deep. Its width is 1.27 m (50 in.). The composite ailerons in L-1011 aircraft are designed with the following goals.

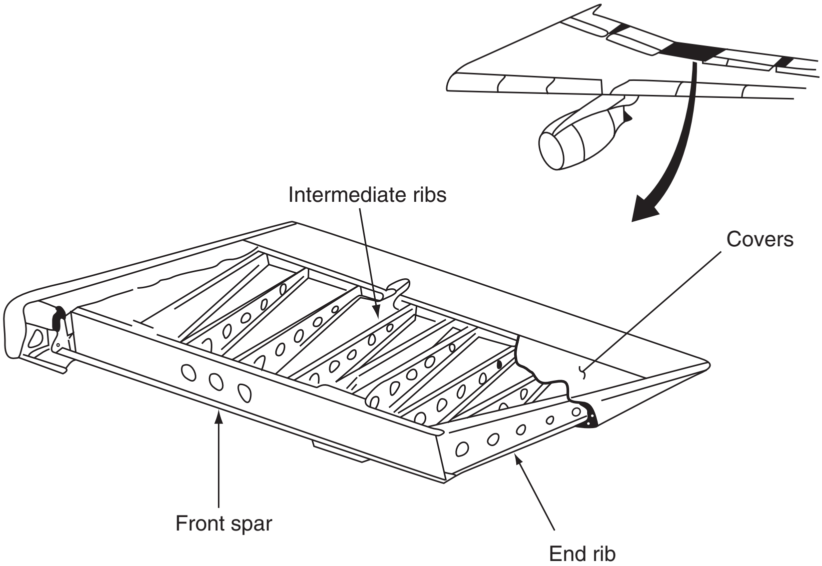

FIGURE 6.20 Construction of a Lockheed L-1011 composite aileron. (*Note*: The hinge and actuator fittings are not shown. They are located on the front spar.)

1. They must directly replace production aluminum ailerons in fit, form, function, and stiffness, and result in weight reduction.
2. As in the case of aluminum ailerons, the composite ailerons must meet the fail–safe design criteria for limit flight loads in accordance with the U.S. Federal Aviation Administration (FAA) requirements.
3. The material selected for the aileron structure must not severely degrade at temperatures ranging from −54°C to 82°C (−65°F to 180°F) or at high humidity conditions.

After careful evaluation of a large number of material as well as design alternatives, the following material and laminate constructions have been selected for the principal structural components of composite ailerons.

Upper and lower covers: The cover panels have a sandwich construction consisting of three layers of T-300 carbon fiber–epoxy tape on each side of a 0.95 mm (0.0375 in.) thick syntactic epoxy core. The laminate configuration is [45/0/−45/syntactic core/−45/0/45], with the 0° plies oriented in the spanwise direction. The syntactic epoxy core is a film epoxy adhesive filled with hollow glass microspheres. Near the main rib as well as at the ends of each cover, the syntactic core is replaced by five plies of T-300 carbon fiber–epoxy tape oriented in the chordwise direction.

Front spar: The front spar is a constant-thickness channel section constructed of a $[45/0/-45/90/0]_S$ T-300 carbon fiber–epoxy tape laminate. The

0° plies in the front spar laminate are in the spanwise direction. Holes are machined in the spar web for access and inspection purposes. The flange width of the spar caps is increased locally to facilitate mountings of main ribs and rib backup fittings.

Main ribs: Main ribs are used at three hinge or actuator fitting locations for transferring loads from the fittings to the aileron covers and spars. They are constant-thickness channel sections constructed with four plies of T-300 carbon fiber–epoxy bidirectional fabric oriented at $[45/90_2/45]$, where 0° represents the lengthwise direction for the rib. Five plies of unidirectional 0° T-300 carbon fiber–epoxy tape are added to the rib cap to increase the stiffness and strength at the rib ends.

Other ribs: In addition to the three main ribs, the aileron assembly has five intermediate ribs and two end closeout ribs that support the covers and share the air pressure load. These ribs are constant-thickness channel sections consisting of five plies of T-300 carbon fiber–epoxy bidirectional fabric oriented at $[45/90/-45/90/45]$, where the 0° direction represents the lengthwise direction for each rib. Five holes are machined in each rib to reduce its weight.

Rear spar: No material substitution is made for the rear spar, since the usage of composites is considered too expensive for the small amount of weight saved over the existing constant-thickness channel section of 7075-T6 clad aluminum.

In the aileron assembly, the upper cover, all ribs, and two spars are permanently fastened with titanium screws and stainless steel collars. The removable lower cover, trailing edge wedge, leading edge shroud, and fairings are fastened with the same type of screws, but with stainless steel nut plates attached to these substructures with stainless steel rivets. To prevent galvanic corrosion, all aluminum parts are anodized, primed with epoxy, and then painted with a urethane top coat. All carbon fiber–epoxy parts are also painted with a urethane coat.

The composite aileron is 23.2% lighter than the metal aileron. It also contains 50% fewer parts and fasteners (Table 6.7). A summary of the ground

TABLE 6.7
Comparison of Composite and Metal Ailerons

	Composite	Aluminum
Weight (lb)	100.1	140.4
Number of ribs	10	18
Number of parts	205	398
Number of fasteners	2574	5253

Source: Adapted from Griffin, C.F., Design development of an advanced composite aileron, Paper No. 79–1807, AIAA Aircraft Systems and Technology Meeting, August 1979.

TABLE 6.8
Ground Tests on Lockheed L-1011 Composite Ailerons

Vibration in the flapping mode	Resonance frequencies comparable with those of metal ailerons
Vibration in the torsional mode	Resonance frequencies comparable with those of metal ailerons
Chordwise static bending stiffness	Composite ailerons 27% less stiff than metal ailerons
Static torsional stiffness	Comparable with metal ailerons
Static loading	124% Design ultimate load without failure at 12° down-aileron positions 139% Design ultimate load at 20° up-aileron positions with postbuckling of the hinge and backup rib webs
Impact loading to cause visible damage at four locations followed by one lifetime flight-by-flight fatigue loading	Slight growth of damage (caused by impact loading) during the fatigue cycling
Simulated lightning followed by static loading	Burn-through and delamination over a small area; however, no evidence of growth of this damage during static testing

Source: Adapted from Griffin, C.F., Design development of an advanced composite aileron, Paper No. 79–1807, AIAA Aircraft Systems and Technology Meeting, August 1979.

tests performed on the aileron assemblies is given in Table 6.8. Additionally, a number of composite aileron prototypes have also been tested on the aircraft during engine run-up, level flights, and high-speed descends. The performance of composite aileron prototypes has been judged equal to or better than the performance of metal ailerons in these tests. As part of the maintenance evaluation program, five sets of composite ailerons were installed on commercial aircrafts and placed in service in September 1981.

6.5.2 Composite Pressure Vessels [38]

Composite pressure vessels with S-glass or Kevlar 49 fiber-reinforced epoxy wrapped around a metal liner are used in many space, military, and commercial applications. The liner is used to prevent leakage of the high-pressure fluid through the matrix microcracks that often form in the walls of filament-wound fiber-reinforced epoxy pressure vessels. The winding is done on the liner, which also serves as a mandrel. The winding tension and the subsequent curing action create compressive stresses in the liner and tensile stresses in the fiber-reinforced epoxy overwrap. After fabrication, each vessel is pressurized with an internal proof pressure (also called the “sizing” pressure) to create tensile yielding in the metal liner and additional tensile stresses in the overwrap. When the proof pressure is released, the metal liner attains a compressive residual

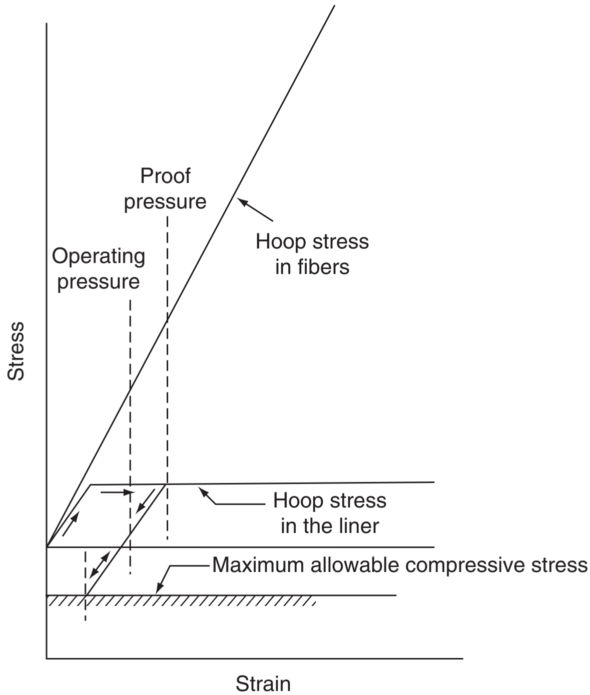

FIGURE 6.21 Schematic stress–strain representations in the composite overwrap and metal liner in a pressure vessel.

stress and the overwrap remains in tension. In service, the metal liner operates elastically from compression to tension and the composite overwrap operates in tension mode (Figure 6.21).

A commercial application of the metal liner–composite overwrap concept is the air-breathing tank that firefighters carry on their backs during a firefighting operation. It is a thin-walled pressure vessel with closed ends containing air or oxygen at pressures as high as 27.6 MPa (4000 psi). The internal pressure generates tensile normal stresses in the tank wall in both the hoop (circumferential) and axial directions. The hoop stress for the most part is twice the axial stress. The fiber orientation pattern in the composite overwrap is shown in Figure 6.22. The metal liner is usually a seamless 6061-T6 aluminum tube with a closed dome at one end and a dome with a threaded port at the other end. The tanks are designed to withstand a maximum (burst) pressure three times the operating pressure. Selected numbers of tanks are tested up to the burst pressure after subjecting them to 10,000 cycles of zero to operating pressure and 30 cycles of zero to proof pressure. Leakage before catastrophic rupture is considered the desirable failure mode during this pressure cycling. Other major

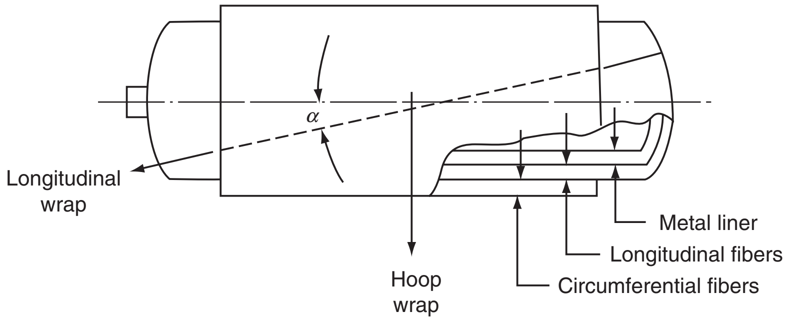

FIGURE 6.22 Fiber orientation in the composite overwrap of a pressure vessel.

qualification tests for the air-breathing tanks are drop impacts, exposure to high temperatures in the pressurized condition, and exposure to direct fire.

6.5.3 Corvette Leaf Springs [39]

The first production application of fiber-reinforced polymers in an automotive structural component is the 1981 Corvette leaf spring manufactured by the General Motors Corporation. It is a single-leaf transverse spring weighing about 35.3 N (7.95 lb) that directly replaces a 10-leaf spring weighing 182.5 N (41 lb).

The material in the 1981 Corvette composite spring is an E-glass fiber-reinforced epoxy with fibers oriented parallel to the length direction of the spring. Although the cross-sectional area of the spring is uniform, its width and thickness are varied to achieve a constant stress level along its length. This design concept can be easily understood by modeling the spring as a simply supported straight beam with a central vertical load P (Figure 6.23). If the

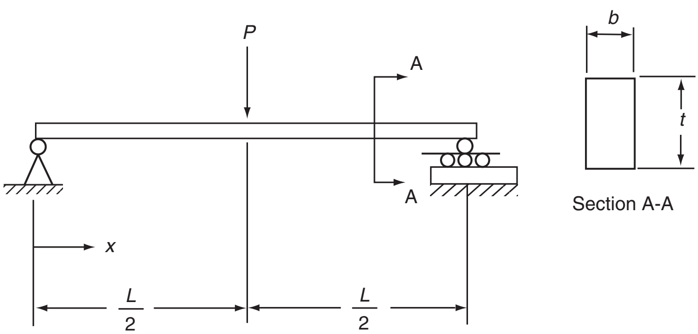

FIGURE 6.23 Simplified model of a leaf spring.

beam has a rectangular cross section, the maximum normal stress at any location x in the beam is given by

$$\sigma_{xx} = \frac{3Px}{bt^2}, \tag{6.38}$$

where b and t are the width and thickness of the beam, respectively.

For a uniform cross-sectional area beam, bt = constant = A_0. Furthermore, the beam is designed for a constant maximum stress, σ_{xx} = constant = σ_0. Thus, using Equation 6.38, we can write the thickness variation for each half length of the beam as

$$t = \frac{3P}{A_0\sigma_0}x \tag{6.39}$$

and correspondingly, its width variation as

$$b = \frac{A_0^2\sigma_0}{3P}\frac{1}{x}. \tag{6.40}$$

Equations 6.39 and 6.40 show that an ideal spring of uniform cross-sectional area and constant stress level has zero thickness and infinite width at each end. The production Corvette composite spring is ~15 mm (0.6 in.) thick by 86 mm (3.375 in.) wide at each end and 25 mm thick (1 in.) by 53 mm (2.125 in.) wide at the center. Two of these springs are filament-wound in the mold cavities, which are machined on two sides of an elliptic mandrel. After winding to the proper thickness, the mold cavities are closed and the springs are compression-molded on the mandrel at elevated temperature and pressure. The pressure applied during the molding stage spreads the filament-wound material in the mold cavities and creates the desired cross-sectional shapes. Each cured spring has a semi-elliptic configuration in the unloaded condition. When the spring is installed under the axle of a Corvette and the curb load is applied, it assumes a nearly flat configuration.

Prototype Corvette composite springs are tested in the laboratory to determine their static spring rates as well as their lives in jounce-to-rebound stroke-controlled fatigue tests. The test springs are required to survive a minimum of 500,000 jounce-to-rebound cycles with a load loss not exceeding 5% of the initially applied load at both high (above 100°C) and low (below 0°C) temperatures. Stress relaxation tests are performed for 24 h at elevated temperatures and high-humidity conditions. Other laboratory tests include torsional fatigue and gravelometer test (to evaluate the effect of gravel impingement on the surface coating). Prototype composite springs are also vehicle-tested to determine their ride and durability characteristics.

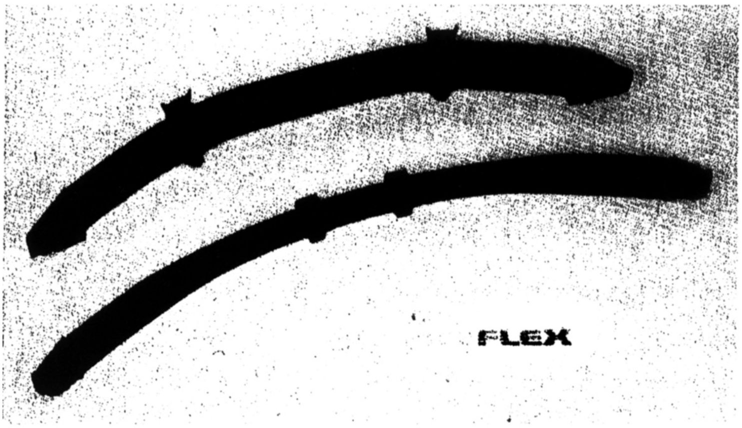

FIGURE 6.24 E glass–epoxy front (*top*) and rear (*bottom*) springs for 1984 Corvette. (Courtesy of General Motors Corporation.)

Figure 6.24 shows photographs of 1984 Corvette front and rear springs made of E-glass–epoxy composite material. The front spring has a constant width, but the rear spring has a variable width. Both springs are transversely mounted in the car. At maximum wheel travel, the front and rear springs support 13,000 N (2,925 lb.) and 12,000 N (2,700 lb.), respectively.

6.5.4 Tubes for Space Station Truss Structure [40]

The truss structure in low earth orbiting (LEO) space stations is made of tubular members with a nominal diameter of 50 mm (2 in.). Lengths of these tubes are 7 m (23 ft.) for the diagonal members and 5 m (16.4 ft.) for other members. The function of the truss structure is to support the crew and lab modules as well as the solar arrays.

The important design criteria for the tubes are

1. Maximum axial load $= \pm 5.33$ kN (± 1200 lb.)
2. Coefficient of thermal expansion $= 0 \pm 0.9 \times 10^{-6}/°C$ (CTE in the axial direction including the end fittings)
3. Low outgassing
4. Joints that allow easy tube replacements while in operation
5. 30 year service life

In addition, there are several environmental concerns in using polymer matrix composites for the space station applications:

1. *Atomic oxygen (AO) degradation*: Atomic oxygen is the major component in the LEO atmosphere. On prolonged exposure, it can substantially reduce the thickness of carbon fiber-reinforced epoxy tubes and reduce their properties. The AO degradation of such tubes can be controlled by wrapping them with a thin aluminum foil or by cladding them with an aluminum layer.
2. *Damage due to thermal cycling*: It is estimated that the space station, orbiting at 250 nautical miles with an orbital period of 90 min, will experience 175,000 thermal cyclings during a 30 year service life. Unless protected by reflective aluminum coatings, the transient temperature variation may range from −62°C to 77°C. In the "worst case" situation, for example, when the tube is always shadowed, the lowest steady-state temperature may reach −101°C.
3. *Damage due to low-velocity impact during assembly or due to extravehicular activities*. This type of damage may occur when two tubes accidentally strike one another or when a piece of equipment strikes the tube. These incidents can cause internal damages in the tube material and reduce its structural properties. They can also damage the AO protective coating and expose the tube material to atomic oxygen.

Since the tubes have large slenderness ratios (length-to-diameter ratios) and are subjected to axial loading, column buckling is considered to be the primary failure mode. Using Euler's buckling formula for pin-ended columns, the critical axial force is written as

$$P_{cr} = \frac{\pi^2 EI}{L^2}, \tag{6.41}$$

where

E = axial modulus for the tube material
I = moment of inertia of the tube cross section
L = tube length

Setting P_{cr} = 5.33 kN, the minimum allowable flexural stiffness (EI) is calculated as 26.49 kN m^2 for the 7 m long diagonal tubes and 13.51 kN m^2 for the 5 m long nondiagonal tubes.

The CTE requirement for the entire tube including its end fittings is $0 \pm 0.9 \times 10^{-6}$/°C. Assuming that the end fittings are made of aluminum and are 5% of the total length, the CTE requirement for the tube is $-0.635 \pm 0.5 \times 10^{-6}$/°C.

Bowles and Tenney [40] used the lamination theory to calculate the axial modulus (E) and CTE for several carbon fiber-reinforced composites. The first three composites are 177°C (350°F) cure carbon fiber–epoxies containing either T-300, T-50, or P-75 carbon fibers (having E_f = 207, 344.5, and 517 GPa, respectively). Two different ply orientations were examined for each of these material systems:

1. $[15/0/\pm 10/0/-15]_S$, containing only small-angle off-axis plies to provide high axial modulus and low CTE
2. $[60/0/\pm 10/0/-60]_S$, containing 60° and −60° plies to provide higher hoop modulus and strength than (1); but lower axial modulus and higher CTE than (1).

A hybrid construction with ply orientations as just described but containing T-50 carbon fiber–epoxy in the ±15° and ±60° plies and P-75 carbon fiber–epoxy in the 0° and ±10° plies was also investigated. For AO protection, thin aluminum foils (0.05 mm thick) were used on both inside and outside of the tubes made of these materials. A 0.075 mm thick adhesive layer is used between the aluminum foil and the composite tube. The fourth material was a sandwich construction with unidirectional P-75 carbon fiber-reinforced epoxy in the core and 0.125–0.25 mm thick aluminum claddings in the skins.

Figure 6.25 shows the axial modulus vs. CTE values for all composite laminates investigated by Bowles and Tenney. It appears that the CTE requirement is met by the following materials/constructions:

1. $[15/0/\pm 10/0/-15]_S$ T-50 carbon fiber–epoxy
2. Both P-75 carbon fiber–epoxy laminates
3. Hybrid construction

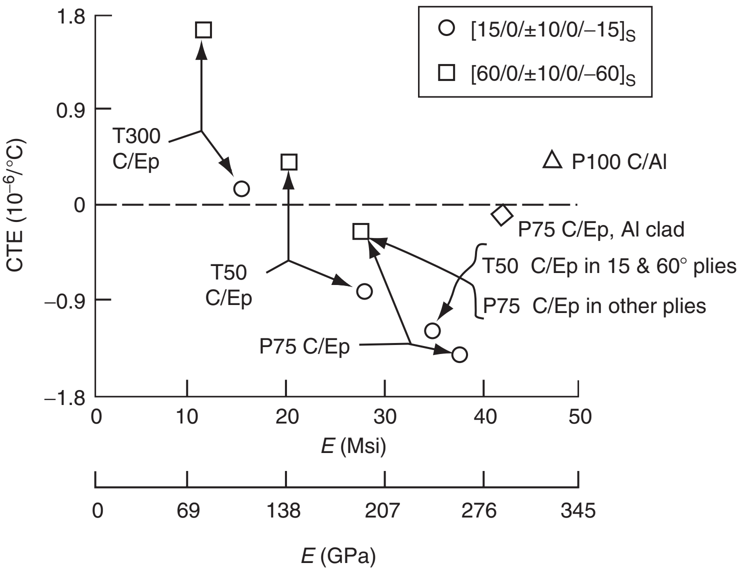

FIGURE 6.25 Axial modulus vs. CTE values for various laminates considered for space station truss structure tubes. (Adapted from Bowles, D.E. and Tenney, D.R., *SAMPE J.*, 23, 49, 1987.)

For comparison, the modulus and CTE values of a P-100 carbon fiber/6061 aluminum alloy composite, also shown in Figure 6.25, are 330 GPa and 0.36×10^{-6}/°C, respectively. The 6061 aluminum alloy has a modulus of 70 GPa and a CTE of 22.9×10^{-6}/°C.

After selecting the laminate type based on the CTE requirement, the next step is to examine which laminate provides the required flexural stiffness and has the minimum weight per unit length. The flexural stiffness EI is a function of the cross-sectional dimensions of the tube. Using an inner radius of 25.4 mm, EI values are plotted as a function of the tube wall thickness in Figure 6.26, along with the range of EI values required for this application. A comparison of tube weight per unit length is made in Figure 6.27, which shows P-75 carbon fiber–epoxy to be the lightest of all candidate materials considered.

Although both $[15/0/\pm10/0/-15]_S$ and $[60/0/\pm10/0/-60]_S$ laminates meet the structural requirements, it is necessary to compare the residual thermal stresses that may be induced in these laminates due to cooling from the curing temperature to the use temperature. These residual stresses can be high enough to cause matrix microcracking, and change the mechanical and environmental characteristics of the laminate.

Figure 6.28 shows the residual thermal stresses in the principal material directions (1–2 directions) through the thickness of a $[15/0/\pm10/0/-15]_S$

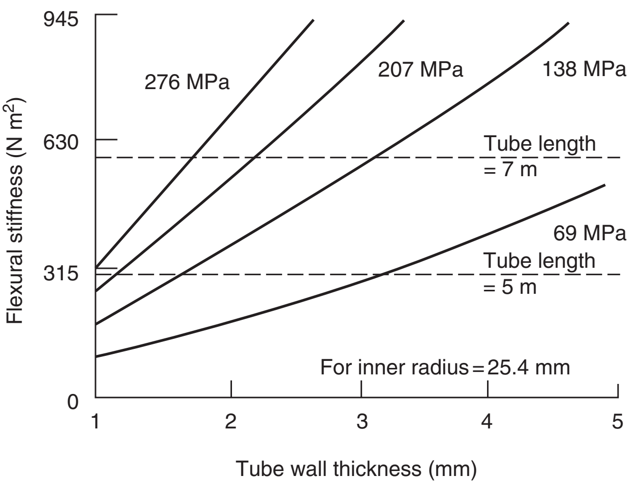

FIGURE 6.26 Flexural stiffness (EI) as a function of the tube wall thickness for different axial modulus values. (Adapted from Bowles, D.E. and Tenney, D.R., *SAMPE J.*, 23, 49, 1987.)

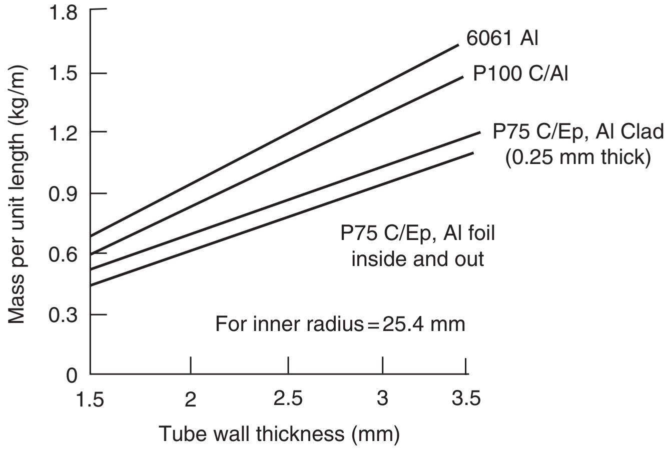

FIGURE 6.27 Mass per unit length of various materials as a function of tube wall thickness. (Adapted from Bowles, D.E. and Tenney, D.R., *SAMPE J.*, 23, 49, 1987.)

laminate. The normal stress σ_{22} (which is transverse to the fiber direction and controls the matrix microcracking) is tensile in all the plies and has the largest magnitude in the 15° plies. A comparison of maximum transverse normal stresses (σ_{22}) in $[15/0/\pm10/0/-15]_S$ and $[60/0/\pm10/0/-60]_S$ laminates indicates that the latter is more prone to matrix microcracking.

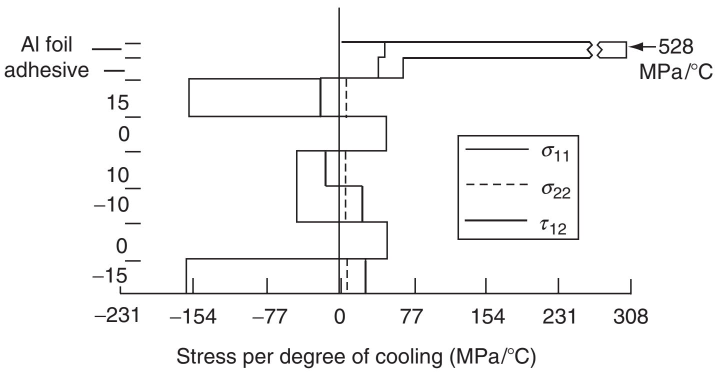

FIGURE 6.28 Thermally induced lamina stresses in a $[15/0/\pm10/0/-15]_S$ carbon fiber–epoxy laminate. (Adapted from Bowles, D.E. and Tenney, D.R., *SAMPE J.*, 23, 49, 1987.)

REFERENCES

1. V.D. Azzi and S.W. Tsai, Anisotropic strength of composites, *Exp. Mech., 5*:283 (1965).
2. S.W. Tsai and E.M. Wu, A general theory of strength for anisotropic materials, *J. Compos. Mater., 5*:58 (1971).
3. E.M. Wu, Optimal experimental measurements of anisotropic failure tensors, *J. Compos. Mater., 6*:472 (1972).
4. S.W. Tsai and H.T. Hahn, Failure analysis of composite materials, *Inelastic Behavior of Composite Materials* (C.T. Herakovich, ed.), American Society of Mechanical Engineers, New York, p. 73 (1975).
5. P.H. Petit and M.E. Waddoups, A method of predicting the non-linear behavior of laminated composites, *J. Compos. Mater., 3*:2 (1969).
6. R.E. Rowlands, Flow and failure of biaxially loaded composites: experimental–theoretical correlation, *Inelastic Behavior of Composite Materials* (C.T. Herakovich, ed.), American Society of Mechanical Engineers, New York, p. 97 (1975).
7. S.R. Soni, A comparative study of failure envelopes in composite laminates, *J. Reinforced Plast. Compos., 2*:34 (1983).
8. R.C. Burk, Standard failure criteria needed for advanced composites, *Astronaut. Aeronaut., 21*:6 (1983).
9. H.T. Hahn, On approximations for strength of random fiber composites, *J. Compos. Mater., 9*:316 (1975).
10. J.C. Halpin and J.L. Kardos, Strength of discontinuous reinforced composites: I. Fiber reinforced composites, *Polym. Eng. Sci., 18*:6 (1978).
11. C.S. Hong and J.H. Crews, Jr., Stress concentration factors for finite orthotropic laminates with a circular hole and uniaxial loading, NASA Technical Paper No. 1469 (1979).
12. B. Pradhan, Effect of width and axial to transverse elastic stiffness ratio on SCF in uniaxially loaded FRP composite plates containing circular holes, *Fibre Sci. Technol., 17*:245 (1982).
13. J.M. Whitney, I.M. Daniel, and R.B. Pipes, *Experimental Mechanics of Fiber Reinforced Composite Materials*, Society for Experimental Mechanics, Brookfield Center, CT (1984).
14. M.E. Waddoups, J.R. Eisenmann, and B.E. Kaminski, Macroscopic fracture mechanics of advanced composite materials, *J. Compos. Mater., 5*:446 (1971).
15. J.M. Whitney and R.J. Nuismer, Stress fracture criteria for laminated composites containing stress concentrations, *J. Compos. Mater., 8*:253 (1974).
16. R.J. Nuismer and J.M. Whitney, Uniaxial failure of composite laminates containing stress concentrations, *Fracture Mechanics of Composites, ASTM STP, 593*:117 (1975).
17. H.J. Konish and J.M. Whitney, Approximate stresses in an orthotropic plate containing a circular hole, *J. Compos. Mater., 9*:157 (1975).
18. J.C. Brewer and P.A. Lagace, Quadratic stress criterion for initiation of delamination, *J. Compos. Mater., 22*:1141 (1988).
19. S.G. Zhou and C.T. Sun, Failure analysis of composite laminates with free edge, *J. Compos. Tech. Res., 12*:91 (1990).

20. H. Kulkarni and P. Beardmore, Design methodology for automotive components using continuous fibre-reinforced composite materials, *Composites*, *11*:225 (1980).
21. J.C. Ekvall and C.F. Griffin, Design allowables for T300/5208 graphite/epoxy composite materials, *J. Aircraft, 19*:661 (1982).
22. M.J. Rich and D.P. Maass, Developing design allowables for composite helicopter structures, *Test Methods and Design Allowables for Fibrous Composites, ASTM STP, 734*:181 (1981).
23. C.T. Herakovich, Influence of layer thickness on the strength of angle-ply laminates, *J. Compos. Mater., 16*:216 (1982).
24. S.L. Donaldson, Simplified weight saving techniques for composite panels, *J. Reinforced Plast. Compos., 2*:140 (1983).
25. T.N. Massard, Computer sizing of composite laminates for strength, *J. Reinforced Plast. Compos., 3*:300 (1984).
26. W.J. Park, An optimal design of simple symmetric laminates under first ply failure criterion, *J. Compos. Mater., 16*:341 (1982).
27. J.M. Whitney and A.W. Leissa, Analysis of heterogeneous anisotropic plates, *J. Appl. Mech., 36*:261 (1969).
28. J.M. Whitney, Bending–extensional coupling in laminated plates under transverse loading, *J. Compos. Mater., 3*:20 (1969).
29. R.M. Jones, H.S. Morgan, and J.M. Whitney, Buckling and vibration of antisymmetrically laminated angle-ply rectangular plates, *J. Appl. Mech., 40*:1143 (1973).
30. O.H. Griffin, Evaluation of finite-element software packages for stress analysis of laminated composites, *Compos. Technol. Rev., 4*:136 (1982).
31. J.R. Eisenmann and J.L. Leonhardt, Improving composite bolted joint efficiency by laminate tailoring, *Joining of Composite Materials, ASTM STP, 749*:117 (1979).
32. L.J. Hart-Smith, Designing to minimize peel stresses in adhesive-bonded joints, *Delamination and Debonding of Materials, ASTM STP, 876*:238 (1985).
33. D.P. Maass, Tubular composite compression members—design considerations and practices, *Proceedings 41st Annual Conference*, Society of the Plastics Industry, January (1986).
34. J.M. Whitney, C.E. Browning, and A. Mair, Analysis of the flexural test for laminated composite materials, *Composite Materials: Testing and Design* (*Third Conference*), *ASTM STP, 546*:30 (1974).
35. J.M. Whitney and J.C. Halpin, Analysis of laminated anisotropic tubes under combined loading, *J. Compos. Mater., 2*:360 (1968).
36. G.J. Simitses, Instability of orthotropic cylindrical shells under combined torsion and hydrostatic pressure, *AIAA J., 5*:1463 (1967).
37. C.F. Griffin, Design development of an advanced composite aileron, Paper No. 79-1807, AIAA Aircraft Systems and Technology Meeting, August (1979).
38. E.E. Morris, W.P. Patterson, R.E. Landes, and R. Gordon, Composite pressure vessels for aerospace and commercial applications, *Composites in Pressure Vessels and Piping* (S.V. Kulkarni and C.H. Zweben, eds.), American Society of Mechanical Engineers, New York, PVP-PB-021 (1977).
39. B.E. Kirkham, L.S. Sullivan, and R.E. Bauerie, Development of the Liteflex suspension leaf spring, Society of Automotive Engineers, Paper No. 820160 (1982).
40. D.E. Bowles and D.R. Tenney, Composite tubes for the space station truss structure, *SAMPE J., 23*:49 (1987).

PROBLEMS

P6.1. A Kevlar 49–epoxy composite has the following material properties: $E_{11} = 11 \times 10^6$ psi, $E_{22} = 0.8 \times 10^6$ psi, $G_{12} = 0.33 \times 10^6$ psi, $\nu_{12} = 0.34$, $S_{\mathrm{Lt}} = 203$ ksi, $S_{\mathrm{Tt}} = 1.74$ ksi, $S_{\mathrm{Lc}} = 34$ ksi, $S_{\mathrm{Tc}} = 7.7$ ksi, and $S_{\mathrm{LTs}} = 4.93$ ksi. A unidirectional laminate of this material is subjected to uniaxial tensile loading in the x direction. Determine the failure stress of the laminate using (a) the maximum stress theory, (b) the maximum strain theory, and (c) the Azzi–Tsai–Hill theory for $\theta = 0°, 30°, 45°, 60°$, and $90°$.

P6.2. The Kevlar 49–epoxy composite in Problem P6.1 has a fiber orientation angle of 45° and is subjected to a biaxial normal stress field ($\tau_{xy} = 0$). Determine the failure stress of the laminate using (a) the maximum stress theory, (b) the maximum strain theory, and (c) the Azzi–Tsai–Hill theory for the normal stress ratios of 0, 1, and 2.

P6.3. Biaxial tension–compression tests on closed-ended 90° tubes (with fibers oriented in the hoop direction of the tube) are performed to determine the normal stress interaction parameter F_{12}, which appears in the Tsai–Wu failure criterion.

The desired stress state is created by a combination of the internal pressure and axial compressive load. In one particular experiment with carbon fiber–epoxy composites, the biaxial stress ratio σ_{11}/σ_{22} was -9. The internal tube diameter was 2 in. and the tube wall thickness was 0.05 in. If the burst pressure was recorded as 2700 psi, determine (a) the axial compressive load at the time of failure and (b) the value of F_{12} for this carbon fiber–epoxy composite.

The following strength properties for the material are known: $S_{\mathrm{Lt}} = 185$ ksi, $S_{\mathrm{Tt}} = 7.5$ ksi, $S_{\mathrm{Lc}} = 127$ ksi, $S_{\mathrm{Tc}} = 34$ ksi, and $S_{\mathrm{LTs}} = 11$ ksi.

P6.4. Average tensile strengths of 15°, 45°, and 60° boron–epoxy off-axis tensile specimens are 33.55, 12.31, and 9.28 ksi, respectively. Determine F_{12} for these three cases using the Tsai–Wu failure theory. Which of the three F_{12} values is in the permissible range? What conclusion can be made about the use of an off-axis tensile test for determining the F_{12} value? The following properties are known for the boron–epoxy system: $S_{\mathrm{Lt}} = 188$ ksi, $S_{\mathrm{Lc}} = 361$ ksi, $S_{\mathrm{Tt}} = 9$ ksi, $S_{\mathrm{Tc}} = 45$ ksi, and $S_{\mathrm{LTs}} = 10$ ksi.

P6.5. A $[0/45]_{8S}$ T-300 carbon fiber–epoxy laminate is subjected to a uniaxial tensile force F_{xx}.

Each ply in this laminate is 0.1 mm thick. The laminate is 100 mm wide. The ply-level elastic properties of the material are given in Example 3.6. The basic strength properties of the material are as follows:

$S_{Lt} = S_{Lc} = 1447.5$ MPa, $S_{Tt} = S_{Tc} = 44.8$ MPa, and $S_{LTs} = 62$ MPa. Assuming that the maximum stress failure theory applies to this material, determine F_{xx} at (a) FPF and (b) ultimate failure.

P6.6. A $[0/90/\pm 45]_S$ T-300 carbon fiber–epoxy laminate is subjected to the following in-plane loads: $N_{xx} = 1000$ lb/in., $N_{yy} = 200$ lb/in., and $N_{xy} = -500$ lb/in. Each ply in the cured laminate is 0.006 in. thick. The basic elastic and ultimate properties of the material are as follows: $E_{11} = 20 \times 10^6$ psi, $E_{22} = 1.3 \times 10^6$ psi, $G_{12} = 1.03 \times 10^6$ psi, $\nu_{12} = 0.3$, $\varepsilon_{Lt} = 0.0085$, $\varepsilon_{Lc} = 0.0098$, $\varepsilon_{Tt} = 0.0045$, $\varepsilon_{Tc} = 0.0090$, and $\gamma_{LTs} = 0.015$. Using the maximum strain theory, determine whether any of the laminas in this laminate would fail at the specified load.

P6.7. If the laminate in Problem P6.6 is subjected to an increasing unaxial load in the x direction, determine the minimum load at which the FPF would occur.

P6.8. Show that, for an isotropic material, Equation 6.8 gives a hole stress concentration factor of 3.

P6.9. Show that the hole stress concentration factor for a 0° laminate is

$$K_T = 1 + \sqrt{2\left(\sqrt{\frac{E_{11}}{E_{22}}} - \nu_{12}\right) + \frac{E_{11}}{G_{12}}}.$$

P6.10. Compare the hole stress concentration factors of $[0/90]_{4S}$, $[0/90/\pm 45]_{2S}$, and $[0/90/\pm 60]_{2S}$ T-300 carbon fiber–epoxy laminates. The basic lamina properties are: $E_{11} = 21 \times 10^6$ psi, $E_{22} = 1.35 \times 10^6$ psi, $\nu_{12} = 0.25$, and $G_{12} = 0.83 \times 10^6$ psi.

P6.11. A 10 mm diameter hole is drilled at the center of the 100 mm wide $[0/45]_{8S}$ laminate in Problem P6.5. Calculate the hole stress concentration factor of the laminate, and state how it may change if (a) some of the 45° layers are replaced with −45° layers, (b) some of the 45° layers are replaced with 90° layers, and (c) some of the 45° layers are replaced with 0° layers.

P6.12. Using the point stress criterion, estimate the notched tensile strength of a $[0/\pm 30/90]_{8S}$ T-300 carbon fiber–epoxy laminate containing a central hole of (a) 0.25 in. diameter and (b) 1 in. diameter. Assume that the characteristic distance d_0 for the material is 0.04 in. The basic elastic properties for the material are given in Problem P6.10. Assume $\sigma_{Ut} = 61$ ksi.

P6.13. Rework Problem P6.12 using the average stress criterion. Assume that the characteristic distance a_0 is 0.15 in.

P6.14. A 300 mm wide SMC-R65 panel contains a 12 mm diameter hole at its center. The unnotched tensile strength of the material is 220 MPa. During the service operation, the panel may be subjected to an axial force of 25 kN. Using a characteristic distance d_0 of 0.8 mm in the point stress criterion, estimate the notched tensile strength of the material and determine the minimum safe thickness of the panel.

P6.15. A T-300 carbon fiber–epoxy panel is made of alternate layers of fibers at right angles to each other. For the various loading conditions shown in the figure, determine the proportion of the two types of layers and their orientations with the x axis. The total laminate thickness may not exceed 0.100 in.

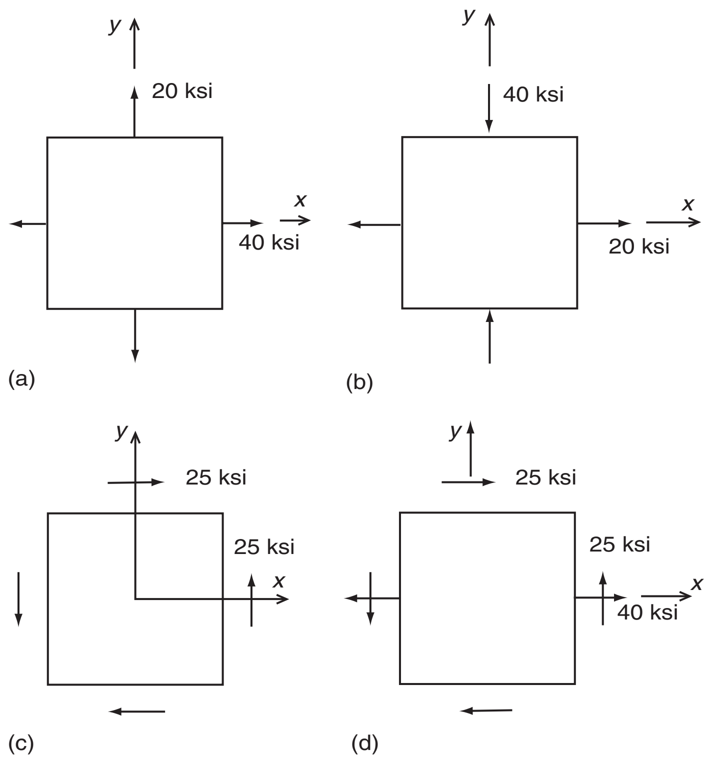

P6.16. The primary load on a rectangular plate, 1 m long × 0.25 m wide, is a 1000 N load acting parallel to its length. The plate is to be made of a symmetric cross-plied T-300 carbon fiber–epoxy laminate with 0°

outside layers. Assuming that the plate is pinned along its width, determine the minimum number of 0° and 90° plies required to avoid failure due to buckling. Each cured layer in the laminate is 0.125 mm thick. Basic elastic properties of the material are given in Appendix A.5.

P6.17. A 20 in. long E-glass–polyester pultruded rod ($v_f = 50\%$) with a solid round cross section is designed to carry a static tensile load of 1000 lb. The longitudinal extension of the rod may not exceed 0.05 in. Determine the minimum diameter of the rod. Laboratory tests have shown that the tensile strength and tensile modulus for the material is 100,000 psi and 5.5×10^6 psi, respectively. Assume a factor of safety of 2.0.

P6.18. A 1 m tension bar of solid round cross section is to be designed using unidirectional GY-70 carbon fiber-reinforced epoxy with 60% fiber volume fraction. The maximum load on the rod is expected to be 445 kN. The rod may be subjected to tension–tension fatigue cycling at an average cycling rate of 10 cycles/s for a total time period of 10 years in an environment where the temperature may fluctuate between −20°C and 100°C. The elongation of the rod should not exceed 0.2 mm.

1. Determine the diameter of the rod using a factor of safety of 3.
2. Assume the rod will be pin-connected at each end to another structure, propose two conceptual designs for the end fittings for the rod and discuss their applicability.

P6.19. A $[0/\pm45/90]_{4S}$ T-300 carbon fiber–epoxy laminate is used in a beam application. Each layer in the cured laminate is 0.005 in. thick. The beam is 0.5 in. wide. Using the basic elastic properties in Problem P6.10, calculate the effective bending stiffness of the laminated beam.

P6.20. Determine the effective bending stiffness and the failure load of a $[(0/90)_8/0]_S$ E-glass–epoxy beam having a rectangular cross section, 12.7 mm wide × 4.83 mm thick. Assume that each layer in the beam has the same cured thickness. Use Appendix A.5 for the basic material properties.

P6.21. A cantilever beam, 0.1 m long × 50 mm wide × 10 mm thick, has a sandwich construction with $[0/\pm45/90]_S$ carbon fiber–epoxy facings and an aluminum honeycomb core. Each layer in the cured laminate is 0.125 mm thick. Assuming that the core has a negligible bending stiffness, determine the end deflection of the beam if it is subjected to a 2000 N load at its free end. Basic ply-level elastic properties of the material are the same as in Example 3.6.

P6.22. A 2 m long, 100 mm wide, simply supported rectangular beam is subjected to a central load of 5 kN. The beam material is pultruded E-glass–polyester containing 60 wt% continuous fibers and 20 wt% mat. Determine the thickness of the beam so that its central deflection does not exceed 70 mm. Laboratory tests have shown that the tensile modulus of the material is 35.2 GPa. Assume its flexural modulus to be 20% less than the tensile modulus.

P6.23. A 30 in. long automotive transmission member has a hat section with uniform thickness. It is connected to the frame by means of two bolts at each end. The maximum load acting at the center of the member is estimated not to exceed 600 lb during its service life. The material considered for its construction is SMC-C20R30.

Modeling the transmission member as a simply supported beam, determine its thickness and the maximum deflection at its center. What special attention must be given at the ends of the transmission member where it is bolted to the frame? The fatigue strength of the SMC material at 10^6 cycles is 45% of its static tensile strength.

P6.24. Using the same material and design requirements as in Example 6.10, design the wall thickness of an automotive drive shaft with a $[\pm 15]_{nS}$ T-300 carbon fiber–epoxy laminate.

P6.25. Design a constant stress cantilever leaf spring of uniform width (70 mm) using (a) E-glass–epoxy and (b) AS carbon–epoxy. Free length of the spring is 500 mm. It is subjected to a reversed fatigue load of ±10 kN. What will be a suitable manufacturing method for this spring?